Published in final edited form as:
Ultrasound Med Biol. 2013 May ; 39(5): 769–783. doi:10.1016/j.ultrasmedbio.2012.11.009.

Patient-Specific Mitral Valve Closure Prediction using 3D Echocardiography

Philippe Burlina[a,b,*], **Chad Sprouse**[a], **Ryan Mukherjee**[a], **Daniel DeMenthon**[a], and **Theodore Abraham**[c]

[a]The Johns Hopkins University Applied Physics Laboratory, Laurel, MD, USA

[b]The Department of Computer Science, Johns Hopkins University, Baltimore, MD, USA

[c]The Johns Hopkins University School of Medicine, Baltimore, MD, USA

Abstract

This paper presents an approach to modeling the closure of the mitral valve using patient-specific anatomical information derived from 3D transesophageal echocardiography (3D TEE). Our approach uses physics-based modeling to solve for the stationary configuration of the closed valve structure from the patient-specific open valve structure, which is recovered using a user-in-the-loop, thin-tissue detector segmentation. The method utilizes a tensile shape finding approach based on energy minimization. This method is used to predict the aptitude of the mitral valve leaflets to coapt. We tested the method using ten intraoperative 3D TEE sequences by comparing (a) the closed valve configuration predicted from the segmented open valve, with (b) the segmented closed valve, taken as ground truth. Experiments show promising results, with prediction errors on par with 3D TEE resolution and with good potential for applications in pre-operative planning.

Keywords

3D echocardiography; pre-operative planning; mitral valve

1. Introduction

The goal of preoperative cardiac surgical planning is to improve quality of repair and decrease patient morbidity and mortality by customizing procedures for an individual patient and evaluating possible outcomes. At present, surgeons and cardiologists have a limited number of tools at their disposal for analyzing patient data and preoperative imagery, and primarily use their experience and case studies to determine the appropriate course of action. The long term goal of our research is to develop methods aimed at improving preoperative planning by allowing a cardiologist or cardiac surgeon to interactively simulate possible surgical corrections and their outcomes. Our work focuses on mitral valve (MV) surgery, which is particularly challenging and could benefit from improved preoperative planning

[*]Corresponding Author: Philippe Burlina, 11100 Johns Hopkins Road, Laurel, MD 20723; philippe.burlina@jhuapl.edu.

tools. This paper presents a method for predicting mitral valve closure based on patient-specific anatomical information derived from 3D TEE.

The mitral valve is a key anatomical structure with a critical function. It is located in the left heart complex, between the left atrium (LA) and left ventricle (LV). The valve consists of an annulus with two leaflets tethered through a complex system of chords (termed *chordae tendineae*) attached to a set of papillary muscles. The papillary muscles are part of the LV inner wall. The MV function is to ensure unidirectional blood flow from LA to LV. For healthy individuals, the valve opens at the beginning of isovolumic relaxation during diastole to allow blood flowing from the lungs to the LA to transfer into the LV. At the start of systole (marking the beginning of isovolumic contraction phase, when the ventricular pressure overcomes atrial pressure), the mitral valve closes, thereby preventing blood backflow (termed *mitral regurgitation* or MR) from the left ventricle back into the left atrium. The prolapse of the mitral valve's leaflets into the atrium is prevented by the retentive action of the chordae tendineae and contraction of the papillary muscles (see Opie, 2004).

The mitral valve's ability to coapt (i.e., form a tight seal) can be degraded (a condition termed *mitral valve insufficiency*), resulting in the regurgitation of blood from the left ventricle back into the left atrium. Regurgitation is a condition that may eventually cause systolic disfunction and congestive heart failure, and thus it is important to diagnose and remedy the condition early. The American Heart Association recommends valvuloplasty, a surgical procedure that involves reshaping the valve apparatus, as the most effective remedial action. The preferential view towards MV repair vs. MV replacement had not always been the prevalent one; the benefits of valve reshaping over valve replacement were brought to light by a set of landmark studies by Carpentier (Carpentier et al., 2010).

Overall, there are a number of surgical options for treating MR, and most involve considerable risks and challenges. A preoperative planning process relying on 3D patient-specific data, obtained *in vivo*, and elucidating which valvuloplasty option is more likely to result in a successful outcome (i.e., a competent valve and correct coaptation without regurgitation) would therefore be a capability of critical importance. The ability to predict valve closure based on patient-specific anatomical structure recovered from 3D TEE as presented here is one step toward this capability.

2. Prior work

Heart modeling efforts can be traced back to the early contributions by Peskin (Peskin and McQueen, 1989). Kunzelman et al. (1993) was one of the first studies to use finite element models for MV simulation. Einstein et al. (2005) and Einstein et al. (2010) are examples of the first MV modeling contributions using coupled FSI (Fluid Structure Interaction). Einstein et al. (2005) used a mitral model immersed in a domain of Newtonian blood, the MV model had anterior and posterior leaflets but did not include other structures such as the left ventricle. The work in Dal Pan et al. (2005) was aimed at evaluating the edge to edge MV repair. Recently, Lau et al. (2010) compared results of MV modeling obtained using 'dry' (structure only) and 'wet' (using fluid and structure) models of the MV. Other notable recent related efforts include Bassingthwaighte (1997), Weinberg and Kaazempur-Mofrad (2006), and Diniz dos Santos et al. (2008). A more complete taxonomy of methods is provided later in the discussion section.

All of the previously cited mitral valve modeling efforts are neither image-based nor patient specific. More recent studies include simulated anatomical models that are partially or fully reconstructed from advanced volumetric imaging modalities. This includes the work by Hammer et al. (2008), who reported a valve closure simulation method using a linear mass-

spring mesh model to predict the MV closure. The anatomy was obtained from ex-vivo porcine MVs using micro-CT, a modality providing high spatial resolution. This method was extended to piecewise linear models in Hammer et al. (2011), which was also a pioneering study in that it performed evaluation using ground truth derived from volumetric imaging. Votta et al. (2008), performed simulations using nonlinear tissue models and an MV apparatus consisting of elementary leaflets but a patient-specific valve annulus derived from 3D echocardiography. Stevanella et al. (2011), in a three patient study, used notional leaflet models but MRI image-derived annuli, pap muscles, and insertion point positions. Krishnamurthy et al. (2009) used radiopaque markers and videofluoroscopy in a study with 10 ovine hearts, utilized finite element models to predict annulus and leaflet properties, and showed that there could be a transient tensing leaflet atrial muscle response explaining the change in annular stiffness. The use of 3D echocardiography, a high temporal resolution modality employed preoperatively and intraoperatively, has now opened the way to performing personalized planning that could be used in a clinical workflow. In Burlina et al. (2010), we reported the first study performing valve closure prediction using patient-specific anatomical valve models (including annuli and leaflets) derived from 3D echocardiography. That study also used a novel shape finding simulation approach. Prot et al. (2010) studied two patient-specific cases of MV, and also performed a modeling study of a porcine MV model of muscle behavior by adding an ac tive contractile component to the MV leaflets (Skallerud et al., 2011). Most recently, Mansi et al. (2012) reported an approach using a dynamic method, linear tissue models, and finite elements and also applied the method on a patient who underwent the MitralClip procedure.

One salient aspect of our proposed approach is that we model the full valve anatomy (an nulus and leaflets) using 3D echocardiography. Despite some challenges, 3D TEE has a number of key advantages for our application when compared to CT and MRI: it is already part of the established clinical cardiology workflow, it has a small form factor, it is non-ionizing, it has lower cost, it can be used both pre- and intraoperatively, and it allows for interactive exploration and diagnostics. A key advantage for cardiac applications, however, is its speed, which is unmatched by other modalities. Current platforms can acquire volumetric images at rates from 20 Hz up to over 50 Hz. Higher rates have been reported in recent commercial platforms. Speed is a key factor when imaging the very rapid motion of the mitral valve, such as the coaptation phase during which the leaflets initially close, which can occur in less than 50 ms.

Another salient aspect in which our approach differs from past work is in the computational method used for valve mechanical modeling. Prior modeling studies – wether patient specific or not - have tended to resort to more complex FEM models or dynamic models that depend on a number of parameters that cannot be measured or easily estimated. In this work, we find the closed valve configuration by solving a shape finding problem using a stationary method and an energy minimization approach.

The present manuscript extends the work in Burlina et al. (2010) with a number of enhancements in the prediction model and the validation methods, including: physiological blood loading forces (with direction along the leaflet surface normals and with physiological pressure); linear elastic forces based on the Saint Venant - Kirchhoff model tuned to approximate the empirical MV leaflets' strain-stress behavior found in May-Newman and Yin (1998) (i.e., we selected the Young's modulus so that the resulting stress would cross May-Newman's mean curve for the equibiaxial case taken at 15% stretch); physiological values for all other entities, and both marginal and basal chordae for modeling; optimized chordal lengths, personalized 124 annulus shapes, and patient-specific annulus deformations between open and closed configurations. For the performance evaluation, we use ten 3D TEE test sequences and present a sensitivity analysis of the effect of chordal length. We also

tie the MV stationary shape finding technique to first principles by using Lagrangian mechanics, to demonstrate that it is a well principled mechanical modeling approach.

The next section describes our approach for recovering the valve anatomy from 3D TEE and predicting the closed valve shape. Section 4 reports experimental evaluation results and Section 5 offers discussions on these results and the challenges and opportunities of such a system when considering clinical deployment.

3. Methods

Overall workflow

The proposed workflow is as follows (Figure 1): (a) the valve anatomy is first recovered via segmentation; (b) a mesh is generated from this segmentation; (c) this mesh is used in a simulation process to predict the closed position from the open position; (d) a parameter estimation process addresses the estimation of the tether lengths; (e) once this is done, the model is ready and the mesh could be modified in a way that would reflect various surgical options, such as the resection of part of a valve leaflet or modifications of the chordae tendineae. The system would then be able to model the closure of the valve mesh for an assumed surgical modification, which would let a clinician assess the degree of leaflet coaptation resulting from that surgical option. The work described in this manuscript is a step towards the capability in (e), and its scope covers all the previous steps with the exception of (e). The method supporting the first step, the recovery of the anatomical structure of the valve and the surrounding heart through segmentation, is explained next.

Segmentation

A 3D segmentation of the MV and surrounding left heart structure is employed to recover the valve's open 3D structure at end diastole that is specific to the patient and used next through mechanical modeling of the valve closure. To find this segmentation, we utilize a user-in-the-loop approach. In a first step, large structures (the lower LA) and fine structures (the valve leaflets) are recovered automatically. In a second step, an expert verifies the segmentation and edits or refines parts to make it more accurate. In a third step, the mesh is created from the segmented valve. For the first step, some options have been proposed recently (e.g., Schneider et al., 2010). For this study we use an approach that combines two ingredients: thin tissue detection and *k*-means.

The thin tissue detector performs an analysis of the disparities of the eigenvalues associated with the local intensity Hessian (as in Huang et al., 2006; Sato et al., 2000).

The input 3D TEE image at end diastole is low-pass filtered, then the structure tensor method is applied. Additionally, *k*-means is applied using two classes corresponding to the valve tissue and blood pool (Duda et al., 1995). The output of *k*-means and the structure tensor are combined (union), and morphology is used to remove noisy responses. The previous segmentation method is applied around a window centered on the valve. The result is then edited by an expert then converted into a mesh used for modeling. The valve modeling is described in the next section.

Lagrangian Modeling of the Mitral Valve System

The method then proceeds along the following steps: a mesh is defined on the leaflets and is generated from the segmentation results as reported in the previous section. The mesh describes the state of the valve system in the open position. Each node of the mesh introduces three degrees of freedom to the problem of finding the final closed configuration. To each node is associated an energy term resulting from external forces (consisting of

blood pressure), internal strain energy, collision energy preventing intersection with other portions of the mesh, and tethering energy created by the chordae tendineae. The total energy of the system is then minimized so as to find the displacement taking the mesh from its open configuration to an equilibrium configuration representing the mesh at closed position. Details are now presented.

We start by modeling the mitral valve system in the context of Lagrangian mechanics to tie the stationary method to first principles. The Lagrangian of a system is expressed as

$$L=\phi_{kin}-\phi_{pot} \quad (1)$$

where the kinetic energy φ_{kin} from each MV mesh node i is

$$\phi_{kin}=\sum_{i,k}\frac{1}{2}m_i\dot{q}_{i,k}^2 \quad (2)$$

The variables $q_{i,k}$ denote the degrees of freedom of the system, i.e. i runs over the nodes in the valve mesh and $k\in\{x, y, z\}$ the coordinates for the position of each node, and the terms $\dot{q}_k$ are their time derivatives. Each triangle facet contributes one third of its mass to each of its three nodes, so that the total mass m_i attributed to each node is equal to one third of the sum of the masses of the nodes adjacent triangular facets. The potential energy is given by

$$\phi_{pot}=\sum_i\phi_i^X+\phi_i^E+\phi_i^T+\phi_i^C \quad (3)$$

where ϕ_i^X is the external energy, ϕ_i^E is the strain energy, ϕ_i^T is the tethering energy, and ϕ_i^C is the collision energy. The expressions for these terms are detailed later. Lagrange's equations are given by

$$\frac{d\left(\frac{\partial L}{\partial\dot{q}_{i,k}}\right)}{dt}-\frac{\partial L}{\partial q_{i,k}}=-\frac{\partial F_{i,k}^{diss}}{\partial\dot{q}_{i,k}} \quad (4)$$

where $F_{i,k}^{diss}$ is the Rayleigh dissipation function for each component, defined by

$$F_{i,k}^{diss}=\frac{1}{2}C\dot{q}_{i,k}^2 \quad (5)$$

An expression directly involving the dissipative force is obtained by considering that

$$F_{i,k}=-\frac{\partial F_{i,k}^{diss}}{\partial\dot{q}_{i,k}}=-C\dot{q}_{i,k} \quad (6)$$

so that Lagrange's equations become

$$\frac{d\left(\frac{\partial L}{\partial\dot{q}_{i,k}}\right)}{dt}-\frac{\partial L}{\partial q_{i,k}}=F_{i,k} \quad (7)$$

The previous equation would be the basis for seeking the closure using a dynamic method taking the valve configuration from end diastole to systole; this possibility is discussed in the discussion section. For our system, the potential energy depends only on q_i since we

have conservative forces. Then the first term in Lagrange's equations only involves the kinetic energy and becomes

$$\frac{d\left(\frac{\partial L}{\partial \dot{q}_{i,k}}\right)}{dt}=M\ddot{q}_{i,k} \quad (8)$$

so that finally

$$M\ddot{q}_{i,k}-\frac{\partial L}{\partial q_{i,k}}=F_{i,k} \quad (9)$$

Considering the system at the stationary position (i.e., at rest, where $\dot{q}=\ddot{q}=0$), Lagrange's equations yield a necessary condition on the gradient of the Lagrangian of the stationary system

$$\frac{\partial L}{\partial q_{i,k}}=0 \quad (10)$$

or alternatively:

$$\nabla_q L=0 \quad (11)$$

The stationary configuration is therefore found as the solution for the problem

$$\mathbf{q}^*=\underset{\mathbf{q}}{\operatorname{argmin}}\left(\phi_{pot}\right) \quad (12)$$

The initial state configuration of the open mesh is used to specify the zero energy point for external (fluid pressure), elastic (strain), and tethering forces. The zero energy point for the collision force preventing mesh intersections is the configuration in which all facets of the mesh are not contacting (more specifically, further apart than a threshold distance δ). The closed state is found as the stationary point determined by solving the above energy minimization problem. The specification of the different additive components for the energy in $\phi_i=\phi_i^X+\phi_i^E+\phi_i^T+\phi_i^C$ are now detailed.

Blood loading energy

Blood loading energy is modeled as

$$\phi_i^X=-p_0\mathbf{n}_i\cdot\mathbf{d}_i \quad (13)$$

where $\mathbf{n}_i$ is the surface normal at node i, p_0 is the blood pressure, and $\mathbf{d}_i$ is the displacement vector of node i.

For each facet on the valve leaflets, the direction of the blood pressure forces is specified to lie along the facet normal pointing toward the atrium. The pressure is set to be 13.3 kPa, or 100 mm Hg, an average value for systolic blood pressure (Opie, 2004).

Strain energy

The leaflets are modeled as membranes. We denote the second Piola-Kirchhoff stress at each facet j by $\mathbf{S}_j$ and the Lagrangian Green strain at each facet by $\mathbf{E}_j$.

The strain energy for each node i is given by

$$\phi_i^E = \frac{1}{2}\sum_{j\in\Lambda_i}\frac{A_j d}{3}\boldsymbol{S}_j\cdot\boldsymbol{E}_j \quad (14)$$

where, for each i, the sum is taken over the set Λ_i of all adjacent facets j containing the node i, A_j denotes the area of the undeformed facet j, and d denotes the membrane thickness. For plane stress, we vectorize the stress and strain tensors as $\boldsymbol{E}=\left(E_{xx}, E_{yy}, \sqrt{2}E_{xy}\right)^T$ and $\boldsymbol{S}_j=\left(S_{xx}, S_{yy}, \sqrt{2}S_{xy}\right)^T$. Our stress-strain relationship uses the hyperelastic Saint Venant-Kirchhoff model

$$\boldsymbol{S}_j=\mathbf{H}\boldsymbol{E}_j \quad (15)$$

where the elasticity matrix **H** of the mesh can be written in terms of the Young modulus of elasticity, E, and the Poisson ratio, ν, as

$$\mathbf{H}=\frac{E}{1-\nu^2}\begin{pmatrix}1 & \nu & 0\\ \nu & 1 & 0\\ 0 & 0 & 1-\nu\end{pmatrix} \quad (16)$$

The numerical values taken for our system are set as follows: the Poisson ratio for the anterior and the posterior leaflets is taken to be $\nu = 0.5$, which is the value for an incompressible material; the Young modulus is set to $E = 100$ kPa for the posterior leaflet and $E = 400$ kPa for the anterior leaflet, to reflect the fact that the posterior leaflet is more pliable than the anterior leaflet, and so as to generate stresses that are consistent with stress obtained at 15% strain for the May-Newman-Yin mean equibiaxial case (see May-Newman and Yin, 1998). The leaflet thickness is taken to be 1 mm. The resulting behavior of the strain-stress function is plotted for different situations and for the anterior leaflets and compared to laws from May-Newman and Yin (1998) and Prot et al. (2007) in Figures 2, 3, 4, and 5. These plots exemplify the stress-strain behavior for several scenarios, including: linear equibiaxial (where stretch occurs equally along the radial and circumferential MV direction), linear off-biaxial (where radial stretch occurs at 1.5 the amount of stretching along the circumferential MV direction), and strip biaxial (where the MV is pre-stretched 15% along the circumferential direction, and the radial stretch then occurs, and vice-versa). As is seen in these plots, the strain-stress relationship in the deformed frame of reference is nearly (but not exactly) linear.

Tethering energy

The tethering energy is used to model the effects of the chordae tendineae, whose function is to restrict the range of motion of the leaflets, thereby preventing prolapse in healthy valves. This energy term is nonlinear and specified as

$$\phi_i^T=\begin{cases}\Phi^t\frac{(|\mathbf{p}_i-\mathbf{q}_i|-r_i)^3}{\rho^3} & \text{if} \quad |\mathbf{p}_i-\mathbf{q}_i|>r_i\\ 0 & \text{otherwise}\end{cases} \quad (17)$$

where Φ^t is the strength of the tethering energy coefficient, $\mathbf{p}_i$ is the position of the displaced node i, $\mathbf{q}_i$ is the position of the point to which node i is tethered, r_i is the chord length, and ρ is the scale of the range dependence of the force.

The numerical values are specified as follows: the strength of the tethering energy coefficient is $\Phi^t = 0.07$ J, and the scale of the range dependence of the tethering force is $\rho =$

0.112 * $E[r]$ mm, where $E[r]$ is the average voxel resolution per side, which in our experiments ranges from 0.4 mm to about 0.8 mm (see experiment section). These numerical values are chosen so as to make the tethers quasi-inextensible. This choice was motivated by observations of tether behavior during surgical interventions.

Collision energy

The collision energy is designed to prevent self intersection of the mesh. We specify the collision energy ϕ_i^C by considering a repulsive force between all facet pairs in the valve system

$$\phi_i^C = \sum_j \sum_k \int_{T_j} d\mathbf{r}_j \int_{T_k} d\mathbf{r}_k e\left(|\mathbf{r}_j - \mathbf{r}_k|\right) \quad (18)$$

In Eq. 18 the outer summation is over all the facets T_j not containing node i, while the inner summation is over all the facets T_k not adjacent to facet T_j. Furthermore, in that same equation, the facet point $\mathbf{r}_j$ (resp. $\mathbf{r}_k$) spans the region of the facet T_j (resp. T_k), while $e(d)$ specifies a repulsive energy dependent on the distance d between the interacting facet points, and is defined as

$$e(d) = \begin{cases} \Phi^C\left(1 - \frac{d}{\delta}\right)^n & \text{if} \quad d<\delta \\ 0 & \text{otherwise} \end{cases} \quad (19)$$

where Φ^C specifies the strength of the repulsive force and the exponent n controls the rapidity of the onset of the force, taken here as $n = 4$. In our experiments, the repulsion energy coefficient was taken as $\Phi^C = 5.7 \times 10^7$ J.m^{-4} and the repulsion range is $\delta = 3E[r]$ with $E[r]$ the average voxel resolution described earlier.

The double summation is only considered between facets which are 'close' to each other, and we use an efficient tree-based range search to restrict the computational impact of this summation. This is an important consideration since the computation of the collision energy is a major contributing factor to total computational load. The range δ specifies the interacting node distance under which the collision force becomes active. Since the double integral term is evaluated by further discretizing points within the facet, this range should be set to a value that is on the order of the smallest distance between the mesh nodes. Therefore, at the final configuration, the remaining gap between colliding/coapting leaflets will be on the order of the mesh facet resolution. The mesh resolution can be tuned down to generate smaller gaps, thereby trading slower convergence for finer precision.

Optimization

The variation of total potential energy is a function of 3N displacement coordinates, where N is the number of free nodes in the valve system. The annulus is manually recovered for each patient's valve and nodes located above the annulus belong to the atrium and are therefore not considered free nodes (they are not included in the energy minimization process). To find the closed positions of the leaflets given the distributed forces and imposed displacements, we find the configuration which minimizes the total energy by using the BFGS (Broyden Fletcher Goldfarb Shanno) quasi-Newton optimization process implemented in the Matlab Optimization Toolbox. The benefits of this approach are to avoid the computation of the Hessian and to alleviate some stability issues related to Newton's methods. Details on convergence and the number of iterations required are provided in the Experiments and Discussion sections.

Annulus deformation

To account for changes in annulus shape between diastole and systole in a way that is patient-specific, an expert first segments both the open and closed state annuli from 3D TEE imagery. Expert annulus segmentations are then converted to NURBS curves, which are used to generate an approximate scaling value that is representative of how much the annulus contracted or expanded between end diastole and begin systole. The entire open state mesh is then deformed according to this scaling value, keeping the undeformed state as the simulation energy reference point for computing strain and stress (i.e., the accrued energy due to the leaflet's stretching resulting from the annulus deformation is taken into account to seek the stationary closed MV configuration). As a result, the annulus facets of the mesh, which remain static during simulation, will more closely resemble their final appearance and location as measured from the 3D TEE imagery. The rest of the mesh that was initially deformed will revert back to its minimal energy state and the leaflets will close as the simulation progresses.

4. Experiments

We now describe details of our modeling validation framework: it consists of using real 3D TEE patient data and computing errors by comparing predicted and actual closed configurations and performing sensitivity analysis on one aspect: the effect of chordal length. [Details are presented now].

Data Acquisition and Cases Studied

We collected intraoperative real-time 3D TEE full-volume data sequences of mitral valves from patients of the Johns Hopkins University's School of Medicine. TEE sequences were acquired under a protocol approved by the JHU Institutional Review Board from patients who gave informed consent. Most of these patients underwent Coronary Artery Bypass Grafting (CABG), and were mostly asymptomatic with regard to mitral valve disease, except for patient number one. TEE acquisition was performed using an iE33 Philips console with an X7-2t probe (Philips Medical Systems, Bothell, WA). The TEE cube sizes were $224 \times 208 \times 208$ voxels, measured along the elevational, lateral, and axial directions[1]. The 3D TEE probe was run at frequencies ranging from 3 to 5 MHz[2]. The spatial resolutions ranged from approximately 0.4 to 0.8 mm. The data was collected intraoperatively using a seven beat breath-hold protocol leading to maximal frame rates close to 50 Hz. Acquisition details about each case are reported in Table 1.

Of all the sequences acquired, only a subset were selected to perform this study. In full 3D mode, the workstation's spatial and temporal resolution is enhanced by collating successive sectors of the 3D frustum, each sector being acquired during a full heart cycle, and the temporal synchronization is achieved by using ECG gating. A breath-hold procedure used to collect our data was intended to minimize artifacts caused by the patient's breathing apparatus. Before acquiring a TEE volume, the anesthesiologist temporarily deactivated the patient's respirator and allowed the patient's chest to steady. The patients selected were mostly asymptomatic with regard to arrhythmia so as to minimize artifacts due to TEE sectors being misaligned in full-volume 3D mode. However, since the patients were still breathing during acquisition, this sometimes resulted in unintended probe motion that

[1]These are the canonical directions for 3D echography: i.e., the axial direction is along the acoustic path and corresponds to the z-axis, and the lateral-elevational plane corresponds to the x-y plane parallel to the plane containing theffechographic transducers.

[2]The iE33 platform does not allow fine selection of the transmit frequency. Instead, the user adjusts the frequency by selecting one of three settings (Penetration, General, and Resolution) that can be set using the "2D Opt" control. Additionally, the actual frequency is not recorded in the DICOM headers, therefore only a range of frequencies can be reported here. The platform supports frequencies from 3-7 MHz.

generated misalignment artifacts between sectors. Our subselection process tried to eliminate those sequences that seemed to be affected by sector misalignment. Additional subselection criteria were that there had to be nearly no cropping of the MV, that the valve apparatus had to be seen almost in its entirety in the 3D TEE frustum. The resolution also had to be sufficient and the imaging conditions with regard to contrast and artifacts had to be reasonably good. A little less than one third of the sequences acquired were eventually retained based on these criteria, which resulted in nine separate sequences corresponding to six different patients. Two of the cases entailed predicting closure from two different open positions in the same sequence (test cases 3 and 4), resulting in a total of 10 test cases. These are presented next. For each test case, Table 1 provides specific information on voxel resolution in mm, depth, frame rate and image quality as rated by a cardiologist.

Methods and Results

Frames in the sequence corresponding to end-diastole and systole were automatically segmented using the method described in Section 3. Results of the preliminary segmentation step, combining *k*-means and structure tensor-based thin tissue detection, applied to 3D TEE cubes, are shown in Figure 6. As previously described, preliminary segmentation was followed by visual inspection and user-in-the-loop correction to edit out errors due to ultrasonic imaging artifacts, and to complete any missing anatomical structures due to self obscuration of the valve or limitations of the TEE field of view (see Figure 7). As a final processing step, the segmented valve was converted to a mesh and the mesh was post-processed by automatically closing any holes, applying nearest neighbor mesh smoothing, and removing non-manifold facets.

The segmented 3D mesh was obtained at a frame corresponding to the open valve position, during diastole, taken at or near the end diastolic point. This was used as the initial configuration for the prediction tool, to predict the configuration of the closed valve. The semi-automatically segmented closed valve was used as ground truth for evaluating the prediction error.

Due to the retentive action of the chordae tendineae, it is expected that the predicted closure will depend on the chordal length, yet chords are not easily distinguished, and therefore this entity is often not easy to estimate from 3D TEE imagery. Therefore, chordal lengths are automatically set based on lengths first computed at end diastole for the open valve, as the distance between the papillary muscle head positions and the insertion points on the valve leaflets. The chordal lengths are then found via optimization by seeking the length scaling factor that minimizes the prediction error (i.e., the error between the valve closure configuration predicted by our system, and the actual closed configuration derived by segmentation at systole).

In our models, the chords included both marginal (also called primary) and basal (also called secondary) chordae tendineae. Marginal chords prevent the leaflet edges from moving into the LA, and the basal chords' retentive action prevents prolapsing of the mitral leaflets. On average, a total of three basal chords and four marginal chords per leaflet were placed manually for each case, by looking for cues of chordal insertions from the TEE data and resulting meshes, or when this was unavailable, by distributing them based on prior anatomical knowledge. This resulted in a total of about fourteen chords per MV. Two papillary muscle heads were manually specified – also based on general anatomical knowledge – for each case (Figure 8 depicts an example papillary muscle and tether configuration). As explained in the previous section, the annuli in open and closed configurations were hand segmented from the 3D TEE frusta, and a dilation (or contraction) factor was computed from the open to closed position, and was subsequently applied to the

open mesh annulus prior to running the simulation so as to reflect a transformation to the closed mesh annulus (see Figure 13).

For those inputs that required manual intervention (chordal attachments, papillary head placement, valve annulus), no attempt was made in this study at exhaustively setting these values so as to get the best error performance. Instead, these were set once and the chordal length optimization/simulation were then run. Similarly, all the mechanical model parameters described in the previous section were set once and remained the same across each case (their values are detailed in the previous section).

Various iterations in computing the closed state are shown for one of the cases in Figure 9. Figure 10 shows close ups of the initial and final computed configurations. Color coded areas correspond to the anterior (red) and posterior (blue) leaflets. Note that the red and blue areas include parts of the attached primary chordae tendineae structure. The yellow area includes the annulus as well as the lower part of the atrium. A movie of the closing valve is shown in Figure 14.

The quantitative evaluation involved measuring the mean absolute error (in mm) between the predicted and ground truth meshes, and results are summarized in Table 2. We also show the error map distribution (in mm) for one of the cases in Figure 11. We compared the predicted closed valve mesh with the actual segmented closed valve mesh, by first registering the two meshes, as was done in Hammer et al. (2011), to adjust for the mostly vertical motion of the annulus during closure, and then computing mesh to-mesh distances. The results reported correspond to the optimal tether length estimation (labeled "(OPT)") and include also, for comparison, the mean error found for the end diastole chordal length of the tether without any further optimization (labeled "(EDCL)").

From Table 2, the mean absolute errors appear to be on the order of the 3D TEE spatial resolution. The magnitudes of errors we find are, in absolute terms, comparable to the results reported in a recent paper by Mansi et al. (2012), who also used 3D TEE, but different finite element model and valve tracking approaches, and where errors are measured in a different fashion (simulated to tracked position discrepancy). The magnitudes of the errors found in this study are also comparable, when looked in relative terms (i.e., when measured in voxels) with the results reported by Hammer et al. (2011), who relied on micro-CT with resolution of about 100 μm and with a modeling method based on linear or piecewise-linear mass-spring models. Such comparisons however should be considered with caution, since results in each respective study were obtained using a number of differing experimental conditions, including different datasets, protocols, imaging setting, and procedures for accounting for errors. More discussions are provided in the Discussion section.

We performed a sensitivity analysis by showing the output of the prediction error for various values of the tether length scaling in Figure 12 for various test cases. In these plots, a scaling value of 1 corresponds to the nominal end diastole chordal lengths, other scaling values of the x-axis correspond to multiplicative factors of the EDCL from 0.6 to 1.4. The plots show that the results depend on the chordal length as was also noted by Hammer et al. (2011). These sometimes exhibit a step-function behavior when the length is below a certain value (as the valve can no longer close). Past this step point, increasing the length usually shows an improvement then a degradation trend occurs. For additional comparisons, the mean absolute prediction errors for the optimized and nominal EDCL lengths are also shown in Table 2.

The results for prediction error computation and sensitivity analysis (see next) were obtained by using meshes with about 1000 facets (and 500 vertices) which took in average about 5 minutes, single threaded, on an i7 workstation. We ran higher resolution examples

consisting of about 4000 facets (2000 vertices) which took about one hour, and large cases with 21000 facets (10000 vertices) which took about a day to complete. The number of iterations ranged from a few hundred (for low resolution) to around a thousand (for high resolutions). No effort was made in this study to improve speed other than utilizing an efficient range search for the collision computation.

5. Discussion and Future Work

In this paper, we have presented a patient-specific method based on using 3D TEE segmentation and modeling to predict the closure of the mitral valve. As explained above, from a quantitative evaluation perspective, preliminary results appear promising. From a qualitative evaluation standpoint, the examination of the closed valve shows closure configurations that appear in agreement with anatomical expectations and are consistent with the fact that most patients had competent leaflet coaptation. Figures 9 and 10 show qualitatively correct valve configurations, and the characteristic shapes of the posterior and anterior leaflets are seen closing along an arc joining the commissure points with a bulge of the leaflets along the mid-area.

Challenges and limitations

This work did not focus on developing and using fully automated leaflet and annulus segmentation and tracking techniques from 3D TEE. Other recent work has already made important contributions with regard to MV and annulus segmentation and tracking (e.g., Schneider et al., 2010; Ionasec et al., 2010). In this study, we have opted instead for a semi-automatic leaflet segmentation and manual annulus segmentation approaches that would minimally interfere with the assessment of the prediction error, and would allow the highest degree of fidelity for the generation of the patient specific valve anatomy. Such user-in-the-loop segmentation and refinement take on the order of 10 minutes per valve. Therefore, we believe that a semi-automated method would be reasonable for clinical use for an initial clinical workflow, as it seems that the 10 minute time investment would be well worth the wait given the high stakes of the procedure.

Nevertheless, despite progress made in the cited literature, challenges still remain in the recovery of the MV anatomy, due to artifacts present in 3D echocardiography, and also due to the complexity of the cardiac anatomy. These challenges have been similarly recognized by other closure prediction studies as potentially limiting current modeling capabilities (see Hammer et al., 2011; Mansi et al., 2012). These are briefly discussed here.

First, it may be difficult to discern in 3D TEE the locations of chordal insertions into the leaflets and more generally where the leaflets end and the chordae tendineae begin. This is partly due to the limitation of the 3D TEE modality and is also somewhat to be expected, as the chordal anatomy consists of intricate extensions of the valve's extremities, and both structures are made of similar types of tissue that are rich in collagen and elastin fibers. Another challenge entails the evaluation of chordal length. This problem is also due to the limitations of the 3D TEE imaging modality as chordae tendineae can only be partially observed. The location of papillary muscles may also be difficult to discern in 3D TEE. In our study, papillary muscle placement was performed manually based on prior anatomical knowledge. The insertion points were also specified manually, based on visual cues (other cited studies of 3D TEE based patient specific modeling used arbitrary insertion points, such as Votta et al. (2008), where these were evenly distributed along the leaflet edge). The chordal length was estimated using a prediction error minimization process. This also serves as a way to mitigate the error caused by arbitrary insertion points and papillary muscle placement, since the distance between the two is taken as a basis for a first estimate of EDCL. For those features that were set manually (papillary muscles and chordal insertions)

we did not attempt exhaustive tuning and optimization. Future work should involve fine characterization and sensitivity analysis of the incidence of setting these entities.

Despite the above cited challenges, 3D TEE currently constitutes the best clinical imaging modality (and the only one allowing real time aquisition) to generate patient specific anatomical information to perform personalized modeling of the MV, for the many reasons that were discussed in the introduction, and some of the imaging limitations mentioned earlier might be offset by future improvements in 3D echocardiography

Constitutive models

Most studies in patient-specific MV simulation, with the exception of Votta's, have thus far used linear (or piecewise linear) strain-stress relationships. This paper uses the hyperelastic Saint Venant-Kirchhoff model (a quasi-linear elastic model), which was tuned to approximate May-Newman's mean equibiaxial hyperelastic stress-strain MV characteristics for the 15% stretch point (May-Newman and Yin, 1998). It is possible that the linear assumption may provide a sufficient first order account for valve stretching (see Dal Pan et al., 2005), and clearly recent related studies have had good success (i.e., reasonable prediction errors) using linear (Mansi et al., 2012) or piecewise-linear (Hammer et al., 2011) models. However, there is also evidence from empirical studies that hyperelastic models are more apt at capturing the behavior of valve tissues (May-Newman and Yin, 1998).

The characterization of the constitutive mechanical properties of valve leaflets is an important and ongoing field of study which has been driven by work in modeling as well as in empirical characterization. Notable contributions include Prot et al. (2007), Sacks and Yoganathan (2007), May-Newman and Yin (1998), Sacks et al. (2002), Grashow et al. (2006), Weinberg and Kaazempur-Mofrad (2006) and Chen et al. (2004). The valve leaflets are soft and hydrated tissues whose constitutive elements include collagen fibers, elastin and glycosaminoglycans (see Kunzelman et al., 1993; Votta et al., 2008), which explain their hyperelastic behavior at the macroscopic level.

Consequently, as an extension of this work we have started investigating (see Sprouse et al., 2011) the integration of a hyperelastic and anisotropic model inspired by the work of May-Newman and Yin (1998). With a porcine model, the stretch response was found by May-Newman and Yin (1998) to be mainly a function of the first invariant and the strain in the direction of the fibers as represented by the strain's fourth invariant.

$$\phi_i^E = c_0\left(\exp\left[c_1(I_1(\boldsymbol{C})-3)^2 + c_2\left(I_4(\boldsymbol{C})^{\frac{1}{2}}-1\right)^4\right]-1\right) \quad (20)$$

where the first invariant of the strain tensor is defined as the trace of the Cauchy-Green strain tensor, $I_1(\boldsymbol{C}) = \mathrm{tr}(\boldsymbol{C})$ and the fourth invariant of strain is defined as $I_4(\boldsymbol{C}) = \boldsymbol{a}^T\boldsymbol{C}\boldsymbol{a}$ where the fiber direction is given by $\boldsymbol{a}$. As May-Newman Yin's study used porcine samples, another interesting follow-up study should investigate the estimation of patient-specific parameters and resulting sensitivity. Lastly, as we have used average systolic pressure values for our models, the use of patient specific systolic pressure values and resulting sensitivity is another investigative path worth pursuing.

Comparing modeling approaches

A first dichotomy of modeling methods regards the use of elastic (as is done in this study and those recently reported in Burlina et al. (2010); Mansi et al. (2012)) and hyperelastic (such as reported in Votta et al. (2008) and our recent work in Sprouse et al. (2011), and as was also done in MV simulations from Einstein et al. (2005) and Lau et al. (2010)). To the

best of our knowledge, the only examples of patient-specific 3D TEE based hyperelastic MV prediction models have been reported in Votta et al. (2008) and Sprouse et al. (2011). The possibility of doing hyperelastic modeling is a worthy endeavor and was discussed earlier. Another route is the piecewise elastic model chosen by Hammer et al. (2011),.

Another possible taxonomy of past work in MV mechanical modeling consists of discerning between tools exclusively performing structural modeling at the exclusion of blood/fluid modeling (so called "*dry*" *models*) and "*wet*" *models* which include studies concerned with fluid and structure interaction (FSI) or work dealing with the computation of hemodynamics (for a review, see Einstein et al., 2010). The work presented here, as well as the works by Hammer et al. (2011), Votta et al. (2008), Burlina et al. (2010), and Mansi et al. (2012) fall in the first category; our work in Sprouse et al. (2009) and other path-leading works by Einstein et al. (2005) and Lau et al. (2010) fall into the second category. Note that the latter two studies are not patient specific, and that, to our knowledge, all 3D patient specific modeling thus far has involved exclusively dry structure-only models. A question arises as to the need for using a wet model for MV modeling. This question is partially answered in Lau et al. (2010) where the author's opinion is that, if the modeling purpose is to characterize the MV closure configuration, the dry models are most probably sufficient. In essence, a structure-only model will likely provide an answer that is of sufficiently high fidelity without justifying the need to recruit more complex, and therefore sometimes more fragile, wet FSI models. Additional consideration when using wet models concerns the realism of the modeling, with methods modeling the MV immersed in a blood domain offering one possibility (used by nearly all the aforementioned FSI studies) and more realistic, more complex, but also more unstable, adaptive Arbitrary Lagrangian-Eulerian (ALE) meshing techniques offering another option. To date, the latter possibility was investigated in the 2D/patient-specific MV case in Sprouse et al. (2009), but has not been fully investigated in 3D/patient-specific cases.

An additional dichotomy concerns techniques attempting a dynamical modeling of the valve motion (using Equation 7) vs. stationary (also termed quasi-static) techniques looking at finding closure via a stationary point approach (using Equation 11). Our modeling falls in this second category, and is, to our knowledge, unique with regards to MV modeling. This technique was justified from first principles by using Lagrangian mechanics, and it is also related to other endeavors reported in other engineering fields (e.g., Hauville et al., 2004). In contrast, Mansi et al. (2012) use the dynamic approach (Equation 7) during part of the heart cycle, from end diastole to systole, to compute closure. Both methods can be shown to derive from Lagrange's equations introduced earlier, and both are liable to finding local minima – when used to find the closure MV configuration – depending on the tuning of their parameters. The reason for this is that both behave like descent techniques over energy functions which are non-convex. We believe that some of the main benefits of the stationary method used here are in its lower complexity, and the fact that fewer assumptions need to be made and fewer unobservable parameters need to be arbitrarily set compared to a wet model or a dynamic model. For example, for a dynamic method, one will need to decide on the values of parameters such as the dissipative force coefficient (see Equation 6) which will need to be arbitrarily set since they cannot be physically measured. When such values are tuned in an ad-hoc fashion, the result is also likely to be a local minimum that depends on the tuning. One last possibility, not yet investigated in the context of patient-specific modeling, is using a dynamic approach throughout the entire heart cycle. In sum, while we do believe that extensions and comparisons are worth exploring – and we intend to do this as future work – the principle of using the simplest method offering sufficiently high fidelity should also be an important guide in the design of a system that will eventually be deployed clinically. The method we have proposed in this paper offers these characteristics while producing a prediction error that is very promising.

6. Conclusions

In this paper, we propose a novel image-based patient-specific mitral valve closure prediction method which may be used to help characterize the competency of a virtually modified valve. The novelty of our approach is twofold: we exploit prior patient-specific structural information which was derived from semi-automated segmentation of 3D TEE, and we use a novel MV closure modeling based on a stationary method utilizing an energy minimization approach. Results are presented and show the promise of the approach.

Supplementary Material

Refer to Web version on PubMed Central for supplementary material.

Acknowledgments

We wish to thank for valuable discussions and help: Drs. D. Yuh (JHU and Yale/Cardiothoracic Surgery), A. Pinheiro (JHU/Cardiology), J. Gammie (UMD / Cardiothoracic Surgery), E. McVeigh and D. Herzka (JHU/BME), M. K. May-Newman (SDSU), D. Freund (JHU APL), R. Juang (JHU APL, Google) and A. Jorstad (EPFL). The support of the JHU APL and the National Institutes of Health through a grant NIH NHLBI R21HL098765 is gratefully acknowledged. The content is solely the responsibility of the authors and does not necessarily represent the official views of the National Heart, Lung, and Blood Institute or the National Institutes of Health.

References

Bassingthwaighte J. Design and strategy for the Cardionome Project. Advances in Experimental Medicine and Biology. 1997; 430:325. [PubMed: 9330741]

Burlina P, Sprouse C, DeMenthon D, Jorstad A, Juang R, Contijoch F, Abraham T, Yuh D, McVeigh E. Patient-specific modeling and analysis of the mitral valve using 3D-TEE. Information Processing in Computer-Assisted Interventions. 2010:135–146.

Carpentier, A.; Adams, D.; Filsoufi, F. Carpentier's reconstructive valve surgery. MI; Saunders Elsevier: 2010.

Chen L, Yin F, May-Newman K. The structure and mechanical properties of the mitral valve leaflet-strut chordae transition zone. Journal of Biomechanical Engineering. 2004; 126:244. [PubMed: 15179855]

Dal Pan F, Donzella G, Fucci C, Schreiber M. Structural effects of an innovative surgical technique to repair heart valve defects. Journal of Biomechanics. 2005; 3812:2460–2471. [PubMed: 16214494]

Dinizdos Santos N, Gerbeau J, Bourgat J. A partitioned fluid-structure algorithm for elastic thin valves with contact. Computer Methods in Applied Mechanics and Engineering. 2008; 19719-20:1750–1761.

Duda, R.; Hart, P.; Stork, D. Pattern Classification and Scene Analysis. 2nd ed.. John Wiley and Sons, Inc.; 1995.

Einstein D, Del Pin F, Jiao X, Kuprat A, Carson J, Kunzelman K, Cochran R, Guccione J, Ratcliffe M. Fluid-structure interactions of the mitral valve and left heart: Comprehensive strategies, past, present and future. Int. Journal for Numerical Methods in Biomedical Engineering. 2010; 263-4:348–380.

Einstein D, Kunzelman K, Reinhall P, Nicosia M, Cochran R. Non-linear fluid-coupled computational model of the mitral valve. The Journal of Heart Valve Disease. 2005; 143:376. [PubMed: 15974533]

Grashow J, Sacks M, Liao J, Yoganathan A. Planar biaxial creep and stress relaxation of the mitral valve anterior leaflet. Annals of biomedical engineering. 2006; 3410:1509–1518. [PubMed: 17016761]

Hammer P, del Nido P, Howe R. Anisotropic mass-spring method accurately simulates mitral valve closure from image-based models. Functional Imaging and Modeling of the Heart. 2011:233–240.

Hammer PE, Perrin DP, del Nido PJ, Howe RD. Image-basedmass-spring model of mitral valve closure for surgical planning. Proc. of SPIE. San Diego, CA, USA. 2008:69180Q–69180Q–8.

Hauville F, Mounoury S, Roux Y, Astolfi J. Equilibre dynamique d'une structure idealement flexible dans un ecoulement: application a la deformation des voiles. Journées AUM AFM. 2004:2004.

Huang A, Nielson G, Razdan A, Farin G, Baluch D, Capco D. Thin structure segmentation and visualization in three-dimensional biomedical images: a shape-based approach. IEEE Transactions on Visualization and Computer Graphics. 2006; 121:93–102. [PubMed: 16382611]

Ionasec R, Voigt I, Georgescu B, Wang Y, Houle H, Vega-Higuera F, Navab N, Comaniciu D. Patient-specific modeling and quantification of the aortic and mitral valves from 4-Dcardiac CT and TEE. IEEET ransactions on Medical Imaging. 2010; 299:1636–1651.

Krishnamurthy G, Itoh A, Swanson J, Bothe W, Karlsson M, Kuhl E, Craig Miller D, Ingels N. Regional stiffening of the mitral valve anterior leaflet in the beating ovine heart. Journal of biomechanics. 2009; 4216:2697–2701. [PubMed: 19766222]

Kunzelman K, Cochran R, Chuong C, Ring W, Verrier E, Eberhart R. Finite element analysis of the mitral valve. The Journal of Heart Valve Disease. 1993; 23:326. [PubMed: 8269128]

Lau K, Diaz V, Scambler P, Burriesci G. Mitral valve dynamics in structural and fluid-structure interaction models. Medical engineering & physics. 2010; 329:1057–1064. [PubMed: 20702128]

Mansi T, Voigt I, Georgescu B, Zheng X, Mengue E, Hackl M, Ionasec R, Noack T, Seeburger J, Comaniciu D. An integrated framework for finite-element modeling of mitral valve biomechanics from medical images: Application to mitralclip intervention planning. Medical Image Analysis. 2012

May-Newman K, Yin F. A constitutive law for mitral valve tissue. Journal of Biomechanical Engineering. 1998; 120:38. [PubMed: 9675679]

Opie, L. Heart physiology: from cell to circulation. Lippincott Williams & Wilkins; 2004.

Peskin C, McQueen D. A three-dimensional computational method for blood flow in the heart I. Immersed elastic fibers in a viscous incompressible fluid. Journal of Computational Physics. 1989; 812:372–405.

Prot V, Skallerud B, Holzapfel G. Transversely isotropic membrane shells with application to mitral valve mechanics. Constitutive modelling and finite element implementation. Int. Journal for Numerical Methods in Engineering. 2007; 718:987–1008.

Prot V, Skallerud B, Sommer G, Holzapfel G. On modelling and analysis of healthy and pathological human mitral valves: two case studies. Journal of the mechanical behavior of biomedical materials. 2010; 32:167–177. [PubMed: 20129416]

Sacks M, He Z, Baijens L, Wanant S, Shah P, Sugimoto H, Yoganathan A. Surface strains in the anterior leaf let of the functioning mitral valve. Annals of Biomedical Engineering. 2002; 3010:1281–1290. [PubMed: 12540204]

Sacks M, Yoganathan A. Heart valve function: a biomechanical perspective. Philosophical Transactions of the Royal Society B: Biological Sciences. 2007; 3621484:1369.

Sato Y, Westin C, Bhalerao A, Nakajima S, Shiraga N, Tamura S. Tissue classification based on 3d local intensity structures for volume rendering. IEEE Transactions on Visualization and Computer Graphics. 20006

Schneider R, Perrin D, Vasilyev N, Marx G, Nido PD, Howe R. Mitral annulus segmentation from 3D ultrasound using graph cuts. IEEE Transactions on Medical Imaging. 2010 PMID: 20562042.

Skallerud B, Prot V, Nordrum I. Modeling active muscle contraction in mitral valve leaflets during systole: a first approach. Biomechanics and modeling in mechanobiology. 2011; 101:11–26. [PubMed: 20419330]

Sprouse C, DeMenthon D, Gammie J, Burlina P. Patient specific modeling of stress strain for surgical planning and guidance. Proc. Int. Conf. Engineering in Medicine and Biology Society. 2011:2011.

Sprouse C, Yuh D, Abraham T, Burlina P. Computational hemodynamic modeling based on transesophageal echocardiographic imaging. Proc. Int. Conf. Engineering in Medicine and Biology Society. 2009; 2009:3649–3652.

Stevanella M, Krishnamurthy G, Votta E, Swanson J, Redaelli A, Ingels N Jr. Mitral leaflet modeling: Importance of in vivo shape and material properties. Journal of biomechanics. 2011

Votta E, Caiani E, Veronesi F, Soncini M, Montevecchi F, Redaelli A. Mitral valve finite-element modelling from ultrasound data: a pilot study for a new approach to understand mitral function and

clinical scenarios. Philosophical Transactions of the Royal Society A: Mathematical, Physical and Engineering Sciences. 2008; 3661879:3411.

Weinberg E, Kaazempur-Mofrad M. A large-strain finite element formulation for biological tissues with application to mitral valve leaflet tissue mechanics. Journal of Biomechanics. 2006; 398:1557–1561. [PubMed: 16038913]

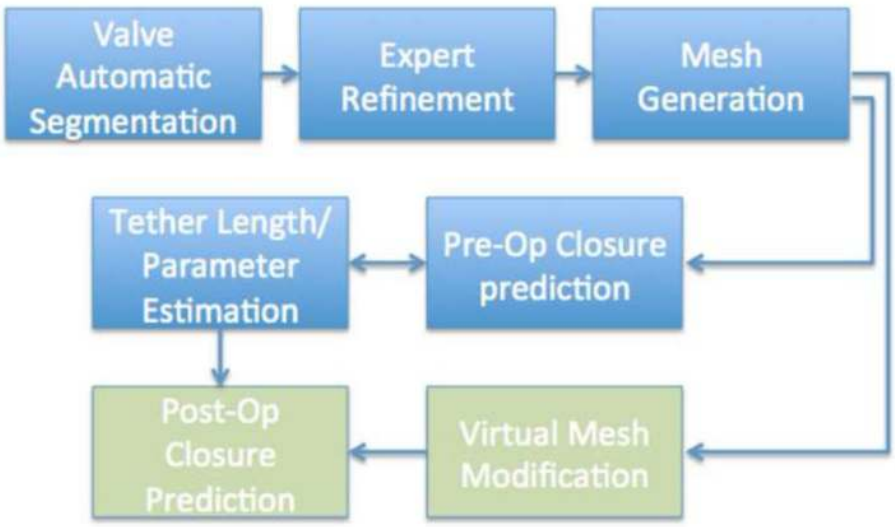

Figure 1.
Flow chart of system studied. The valve anatomy is first recovered via preliminary segmentation using structure tensor and *k*-means. The model is vetted and corrected by an expert for missing or erroneous features. A mesh is created. A parameter estimation process allows the estimation of tether length, which cannot easily be done via imaging only. This consist of finding the chordal lengths that minimize the prediction error between actual and predicted closed configuration. After estimation of the patient specific parameters, the mesh is virtually modified be modified in a way that would reflect possible surgical options and the resulting post-operative closure is predicted. These last processes, indicated in green, are not covered in this manuscript.

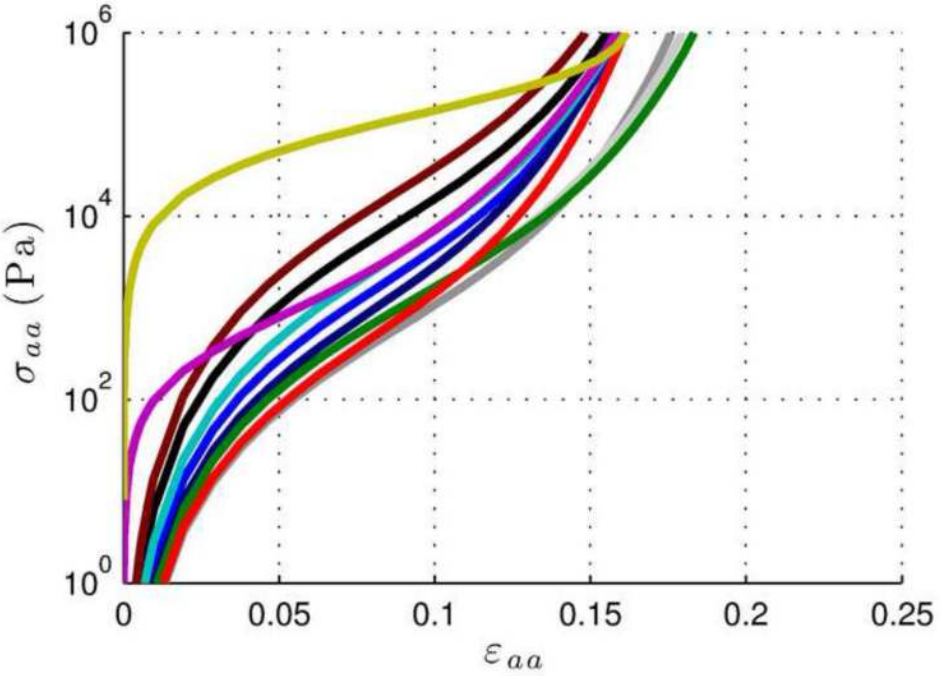

Figure 2.

Our Saint Venant-Kirchho elasticity model (yellow) is tuned to approximate the mean MV behavior (magenta) found empirically in (May-Newman and Yin, 1998) for 15% strain, equibiaxial stretching case (circumferential and radial stretches are equal), anterior leaflet. Stress parallel to the fiber direction (σ_{aa}) is plotted versus strain parallel to the fiber direction (ε_{aa}). Curves represent hyperelastic model with particular parameter sets, May Newman-Yi specimens CP01 through CP08 (black, dark gray, light gray, blue, dark blue, green, red, and dark red respectively), and "mean" (cyan), Holzapfel law (magenta) (Prot et al., 2007)

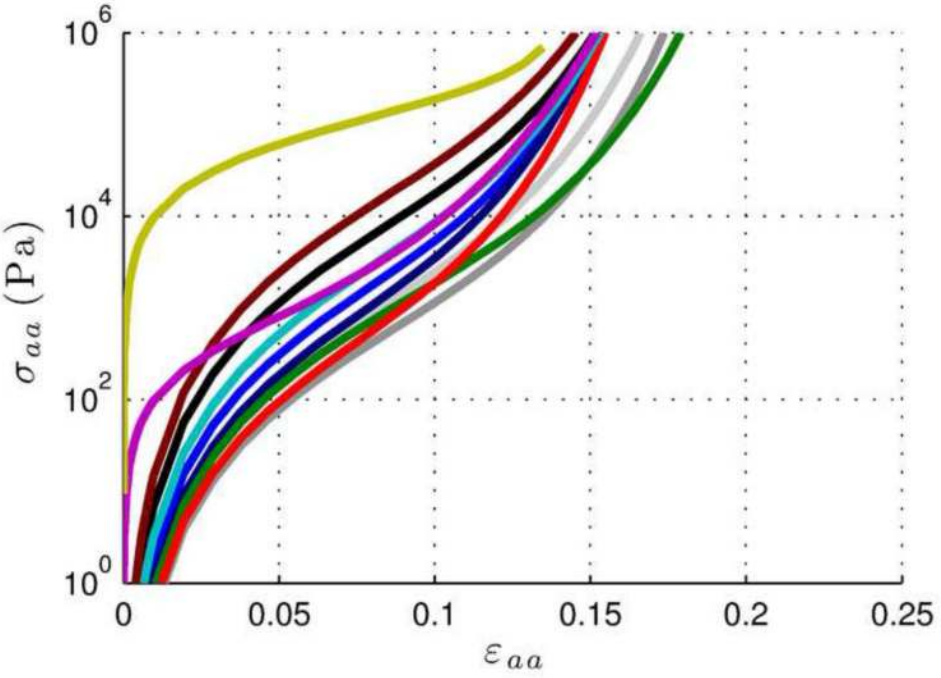

Figure 3.
Elastic stress-strain relationship: off-biaxial case (the MV radial stretch is 1.5 times the circumferential stretch).

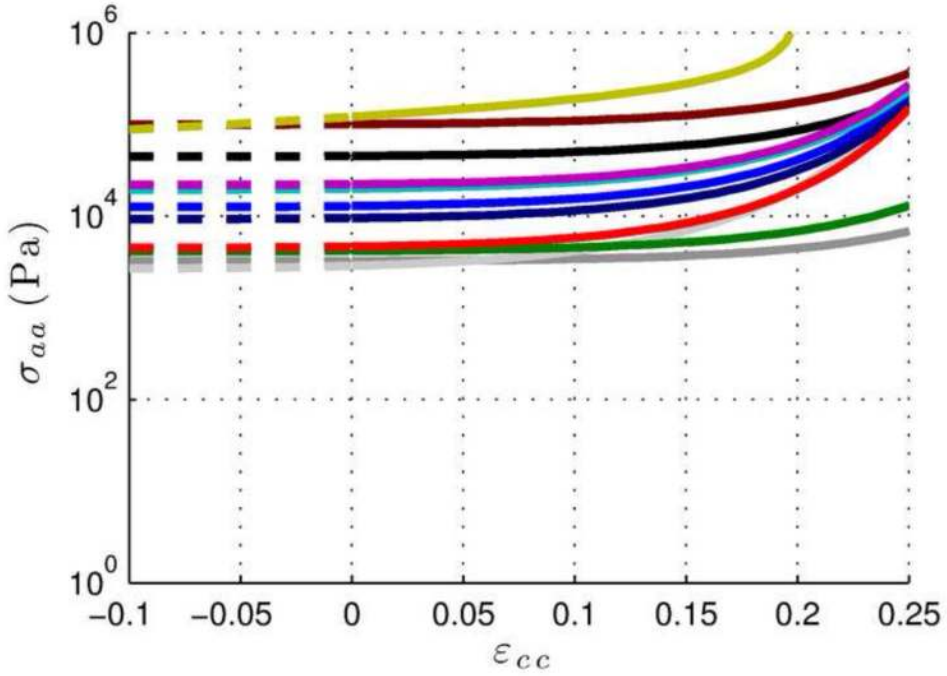

Figure 4.
Elastic stress-strain relationship: strip-biaxial case (the circumferential stretch is fixed at 15% and the radial stretch is varied).

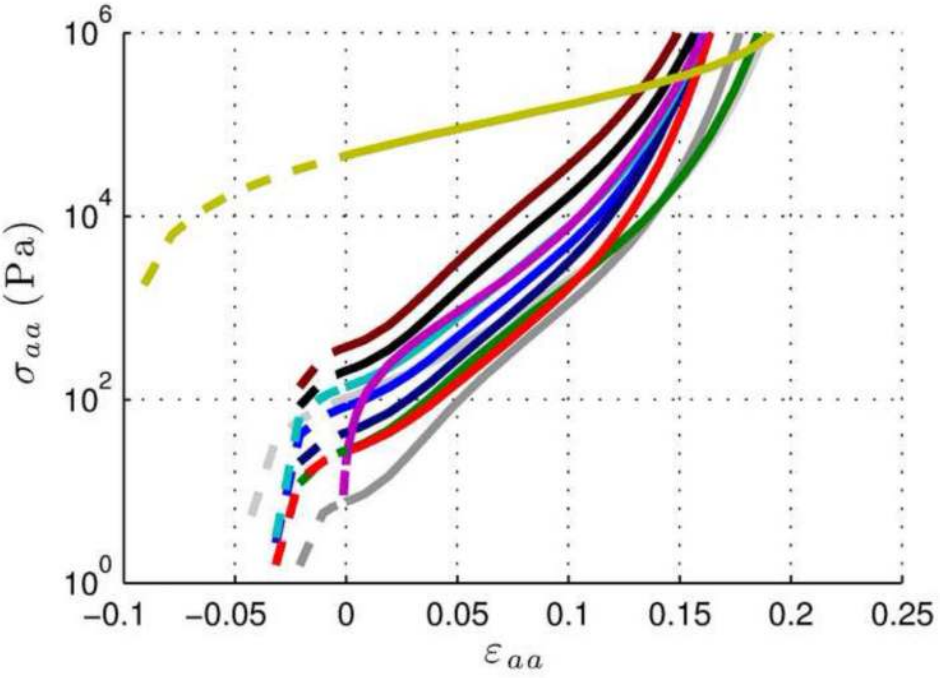

Figure 5.
Elastic stress-strain relationship: strip-biaxial case (the radial stretch is fixed at 15% and the circumferential stretch is varied).

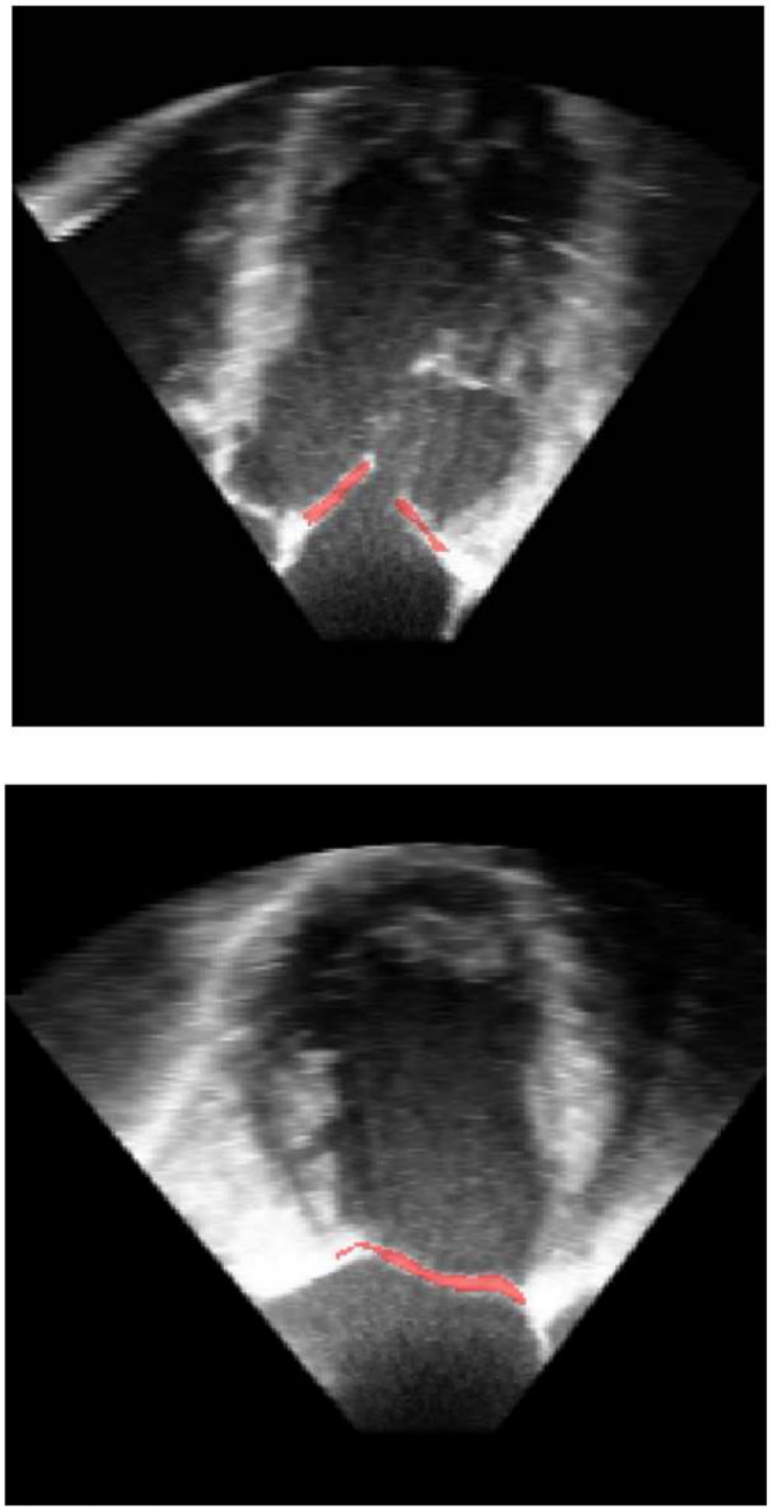

Figure 6.
An exampled of a 3D thin tissue detection of MV leaflets (left) long axis/four chambers view and (right) long axis/two chambers view.

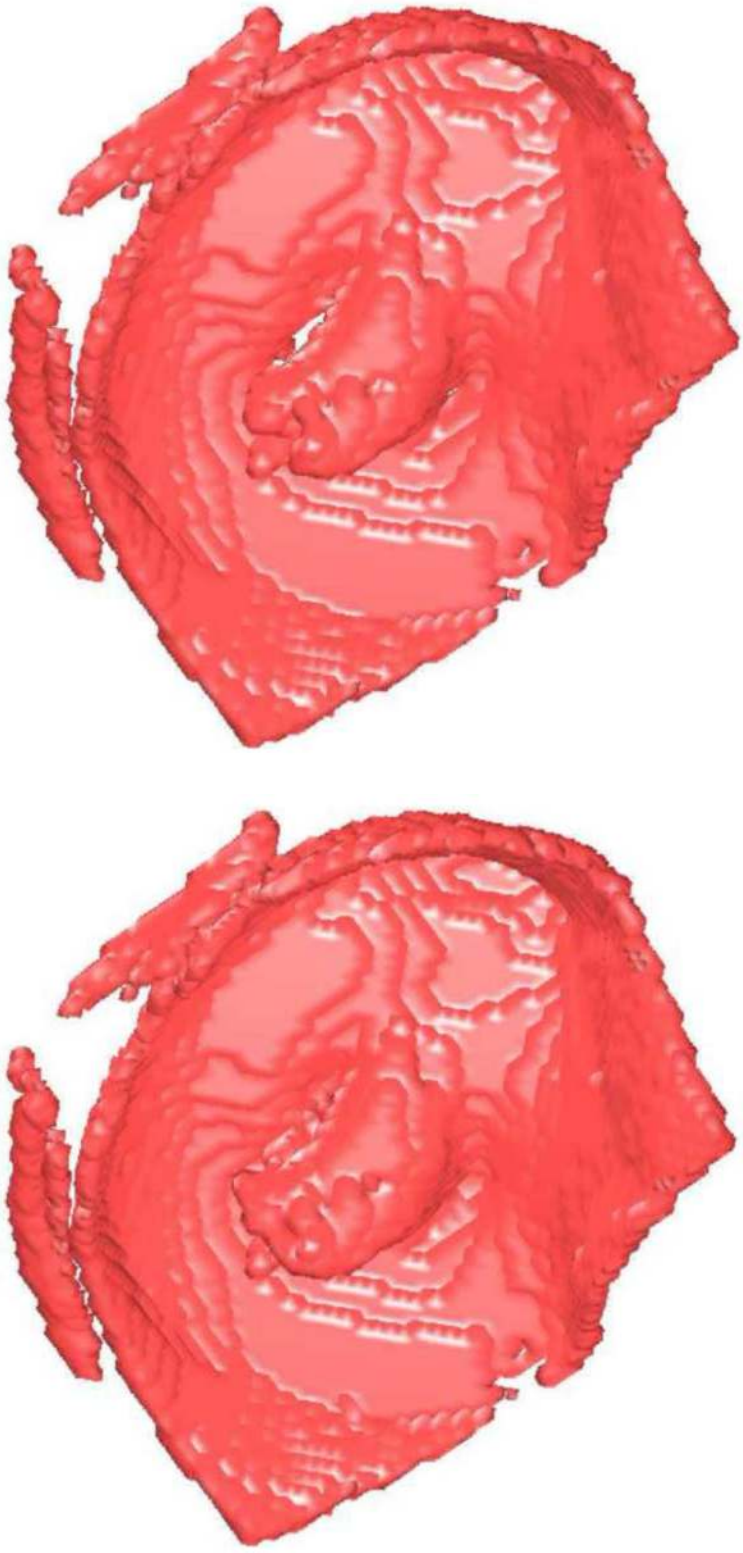

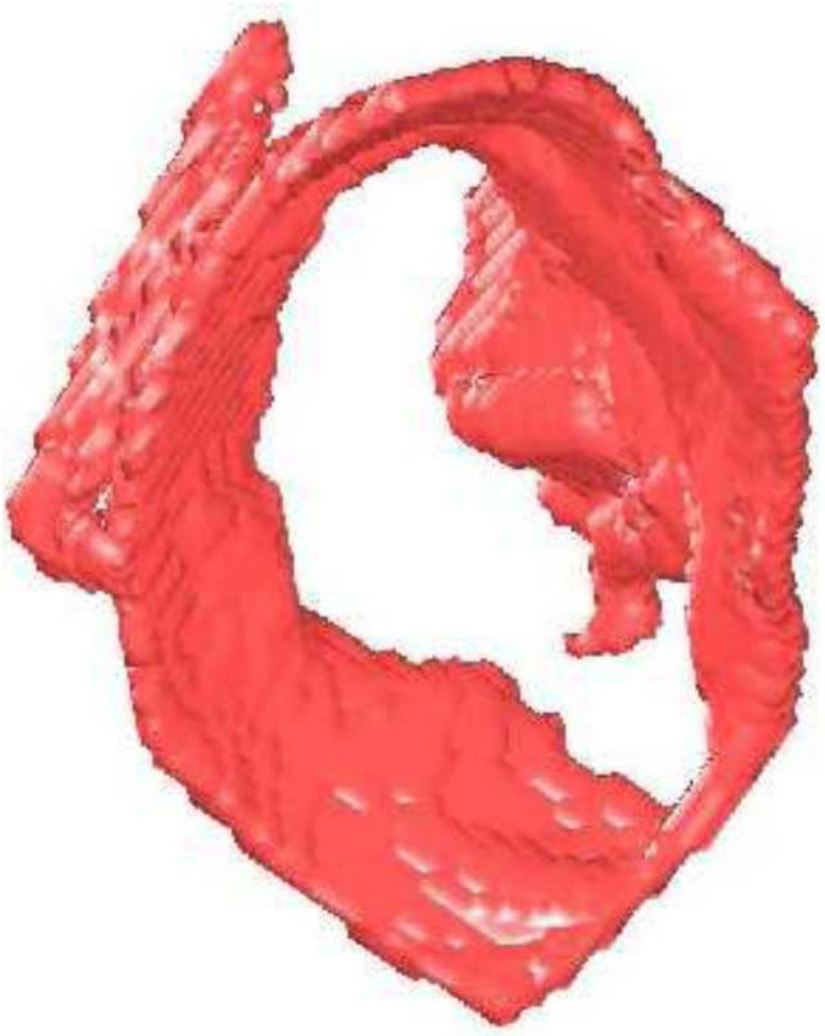

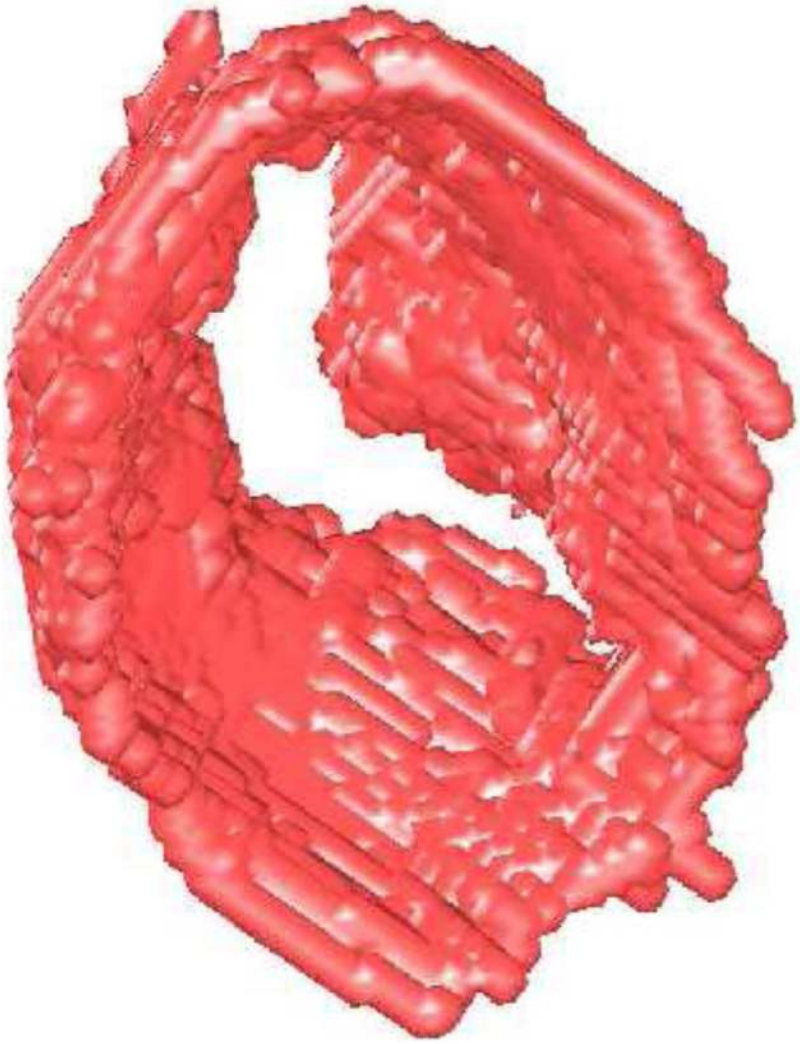

Figure 7.
Examples of segmentation open and closed valve for case 10. (left) output of the preliminary segmentation and (right) after manual semi-automated segmentation.)

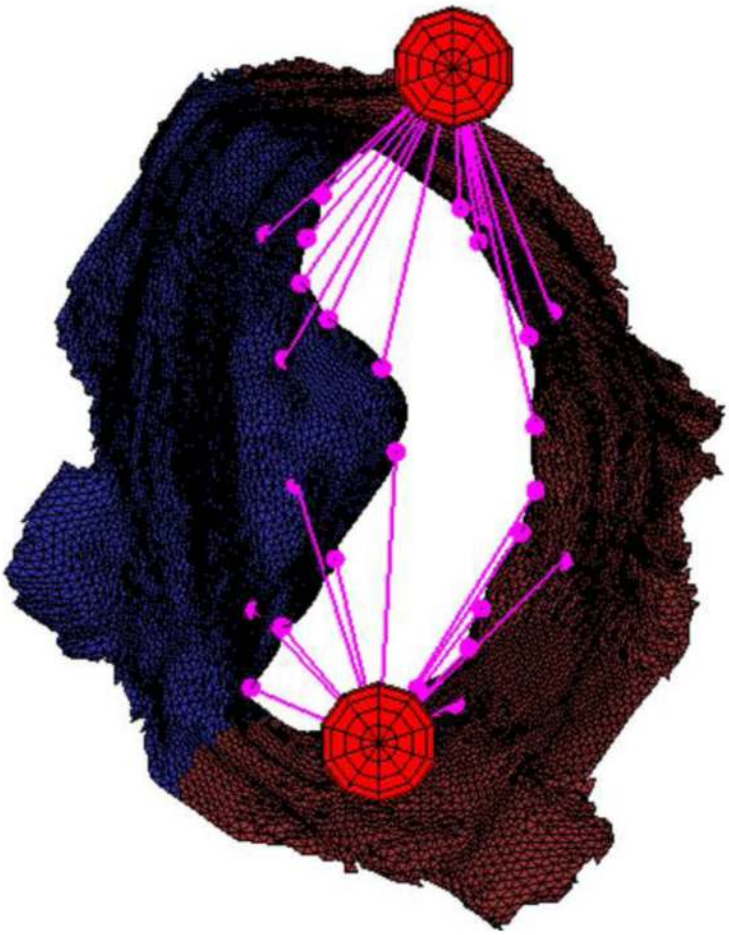

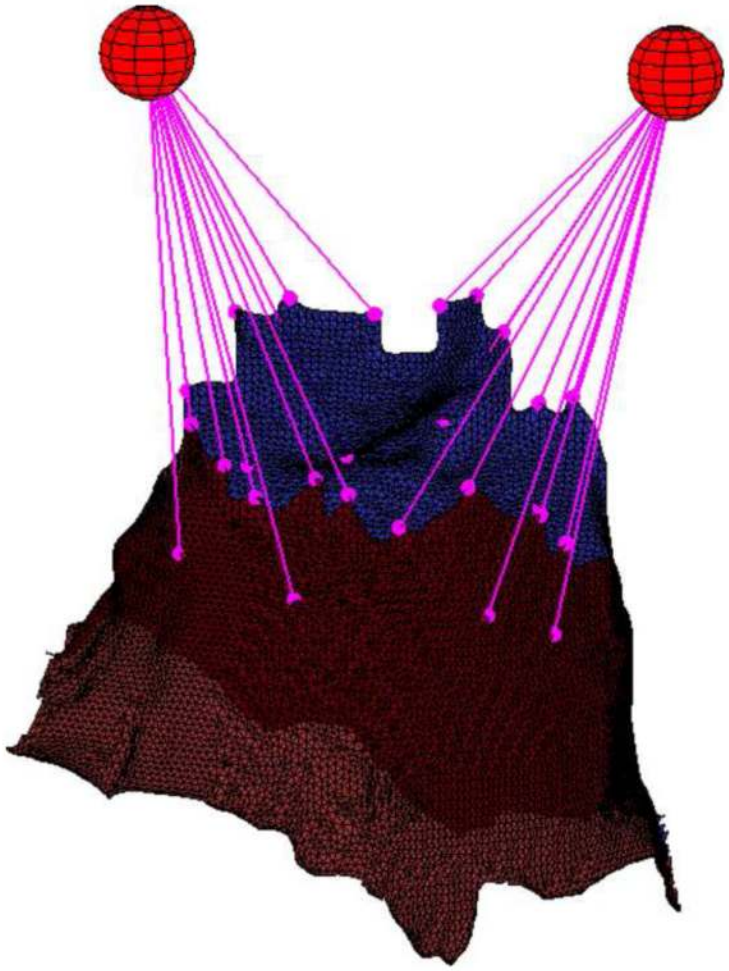

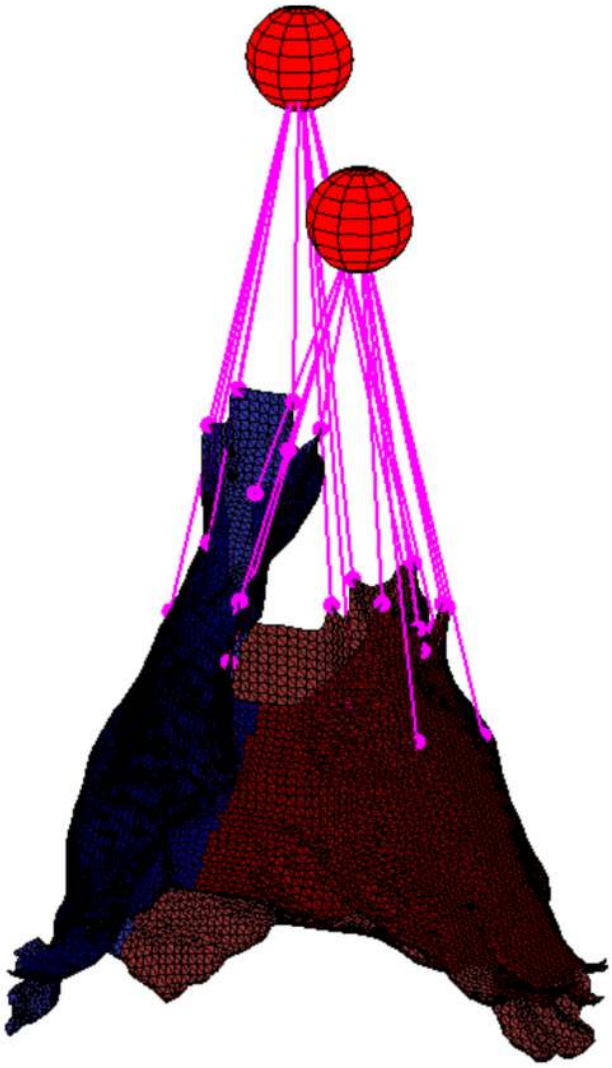

Figure 8.
Example papillary muscle and chordae placement (case 1) from three views: (a) looking up at the mitral valve from within the ventricle, and (b-c) side views of the mitral valve. Papillary muscles are depicted as red balls, chords appear as pink lines, and chordal insertion points are represented as pink dots on the valve mesh. A portion of the annulus and atrium are shown but not clearly marked. Otherwise, the blue portion of the mesh represents the anterior mitral valve leaflet, while the red portion of the mesh represents the posterior mitral valve leaflet. Note that chordae attach to both the tip of the mitral valve leaflets as well as slightly lower on the basal portion of the leaflets; these represent the marginal and basal chordae.

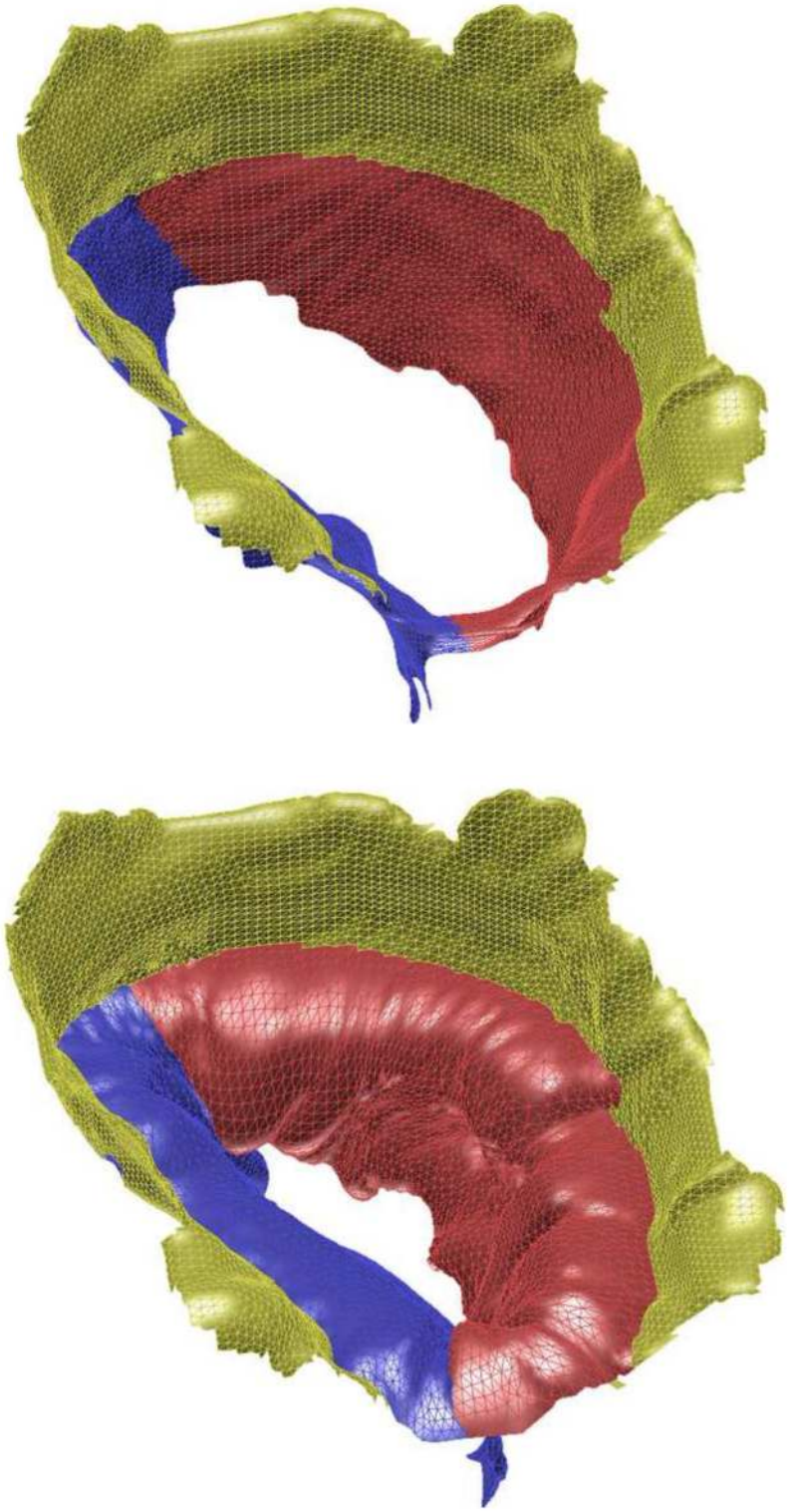

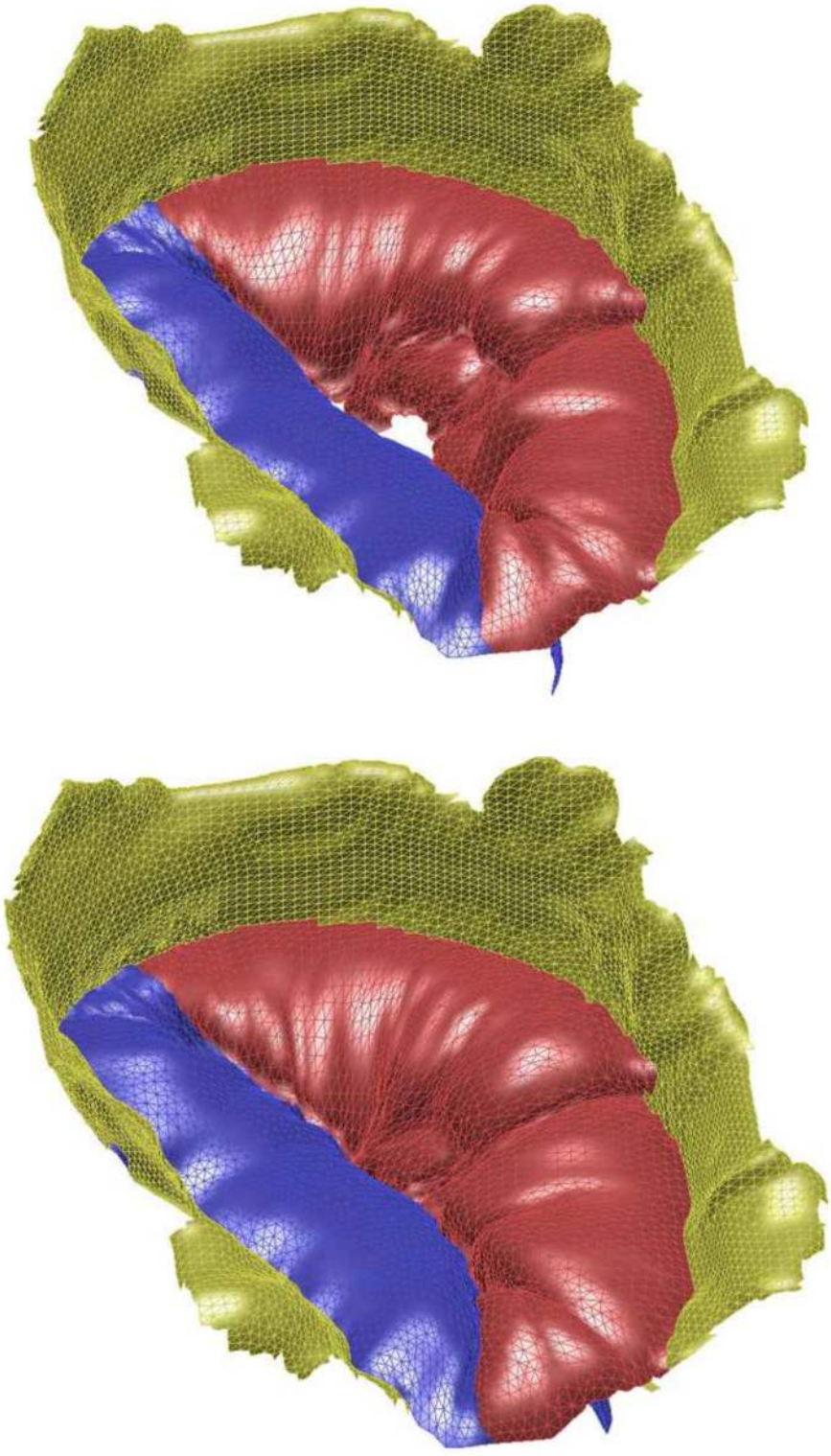

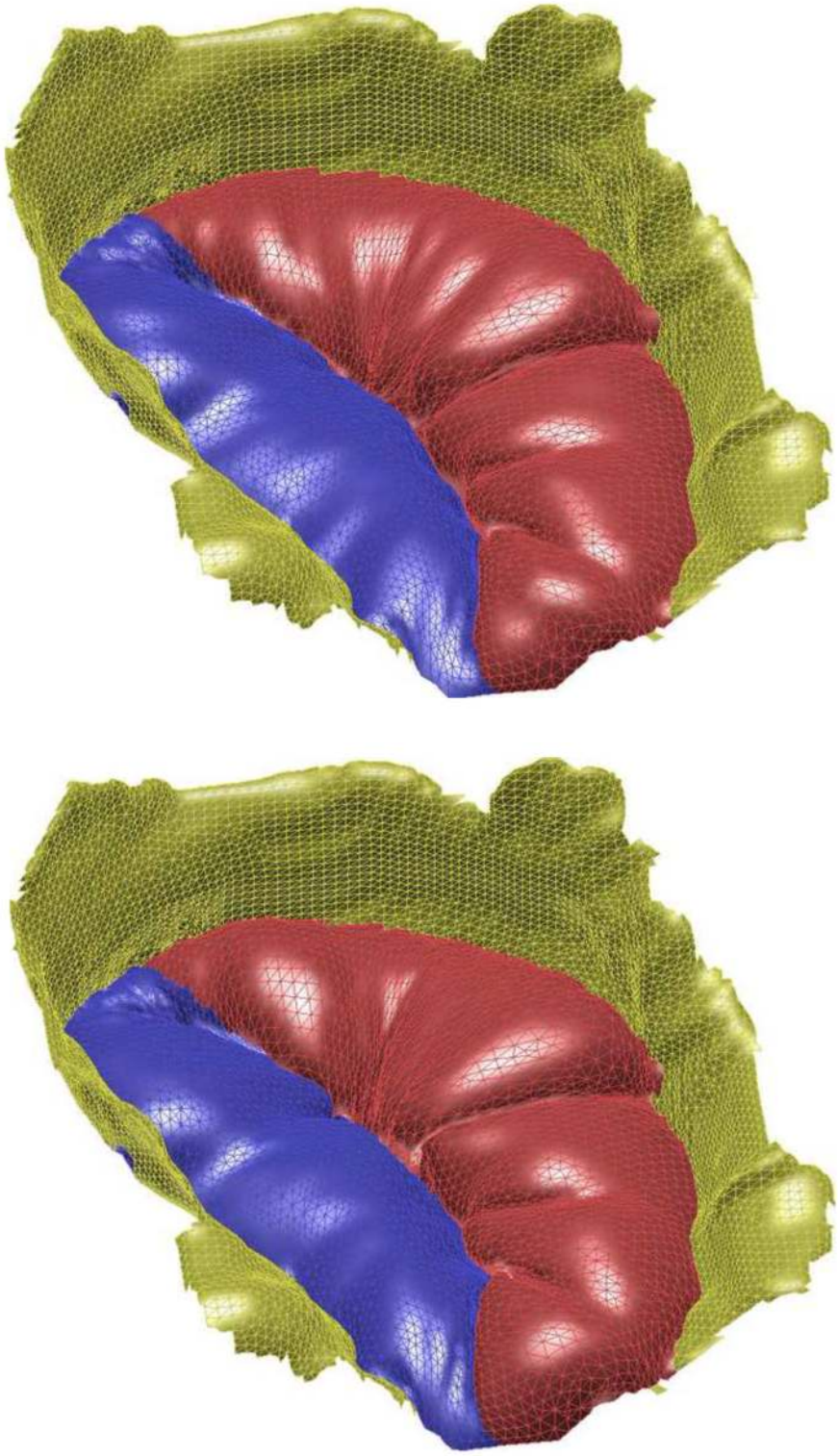

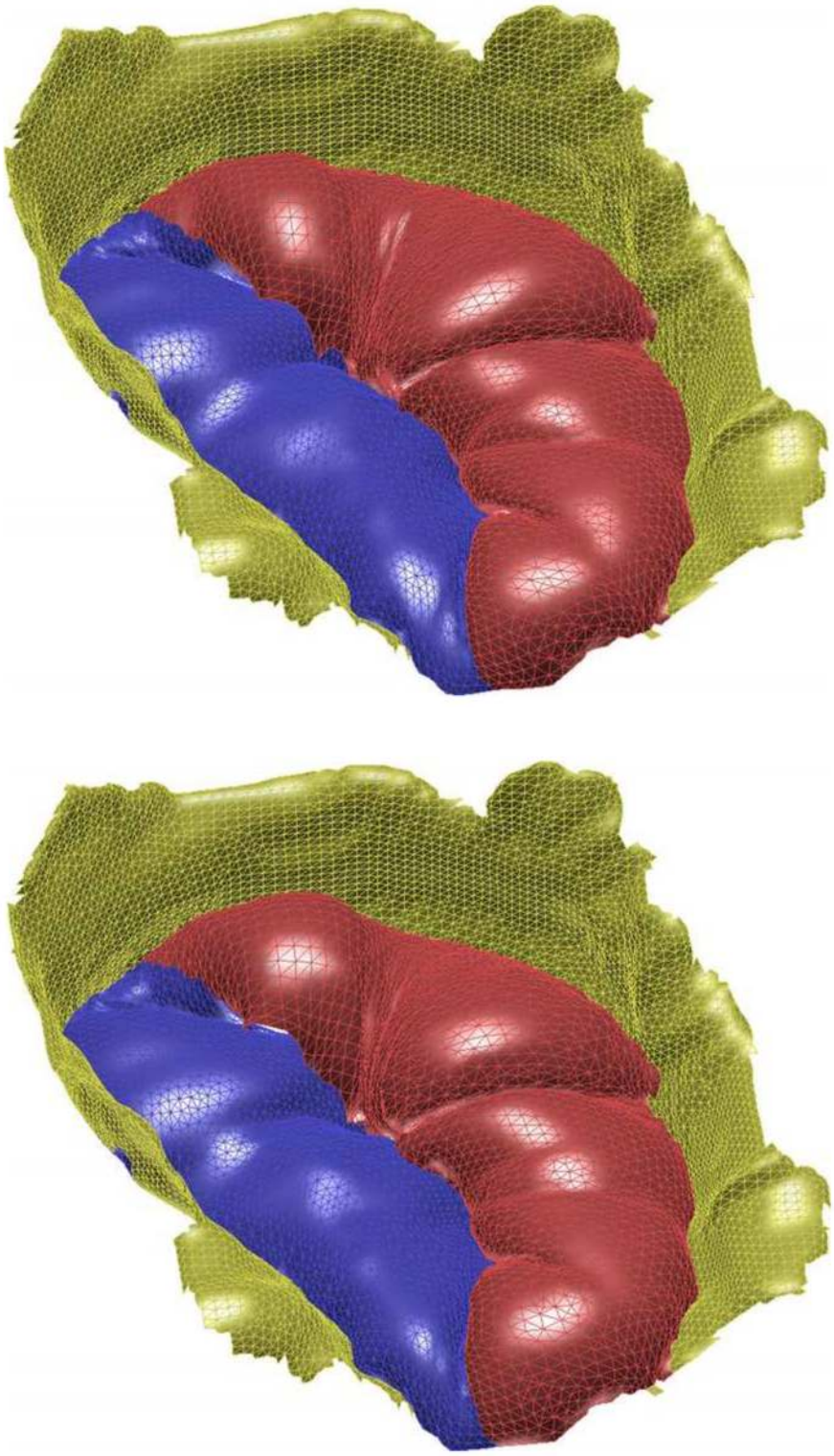

Figure 9.
Sequence of computed configurations taken at various intermediary iterations, top views (case 1).

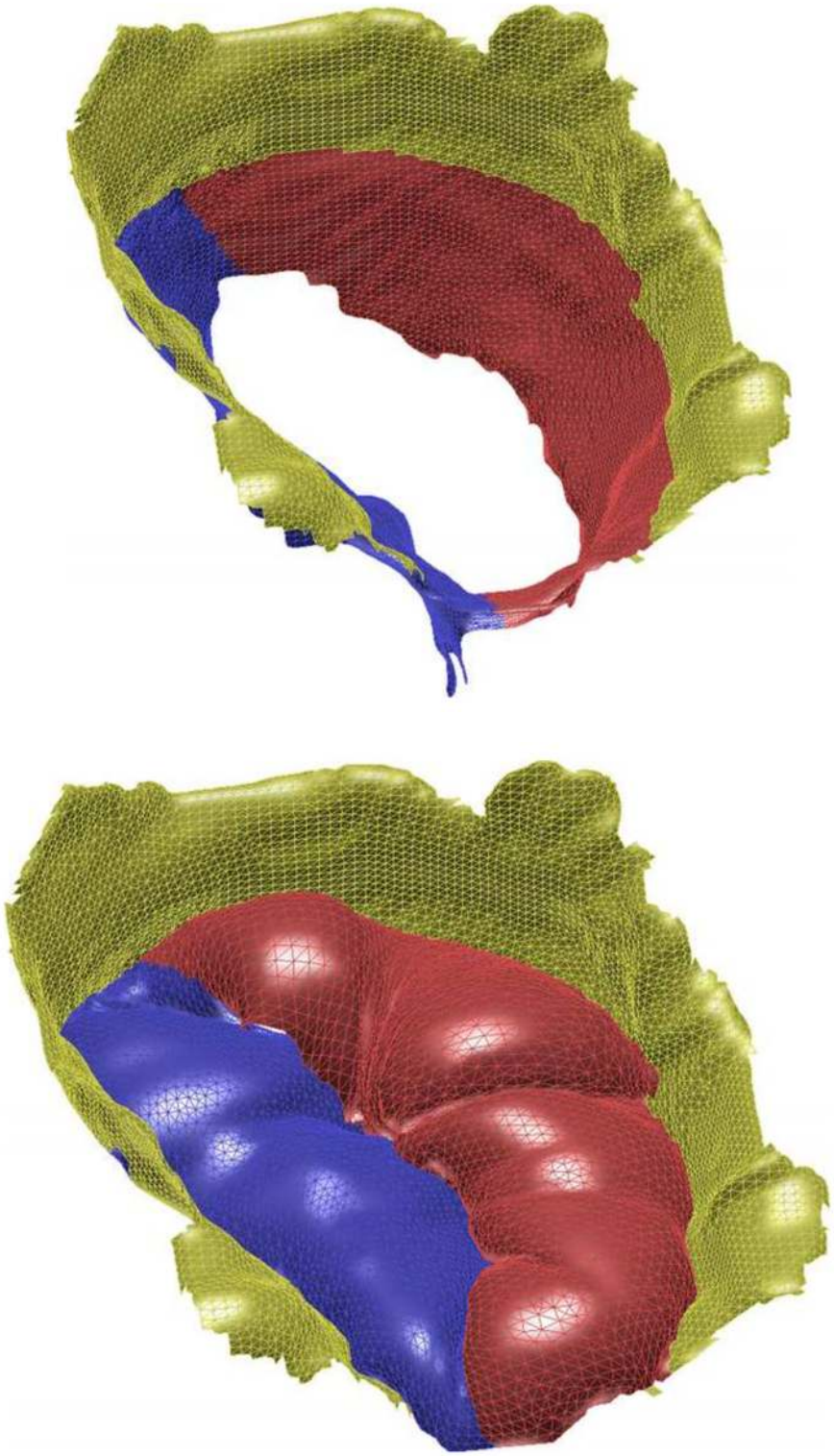

Figure 10.
Initial open valve configuration from TEE segmentation and closed configuration predicted using mechanical modeling (case 1).

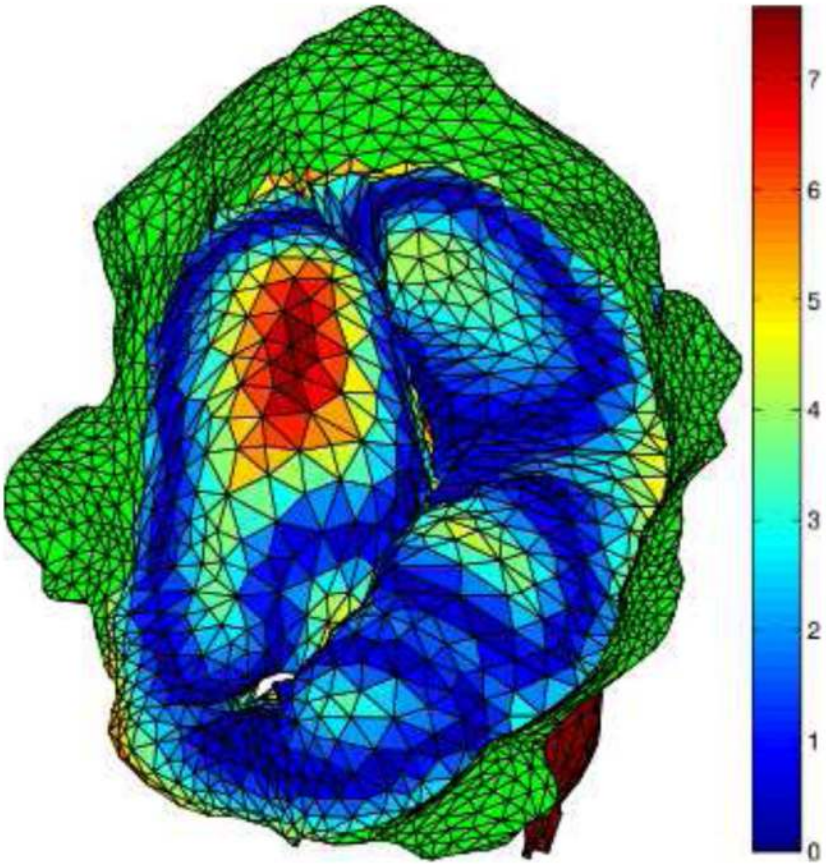

Figure 11.
Error map showing the prediction error distribution (in mm) for the MV (case 1).

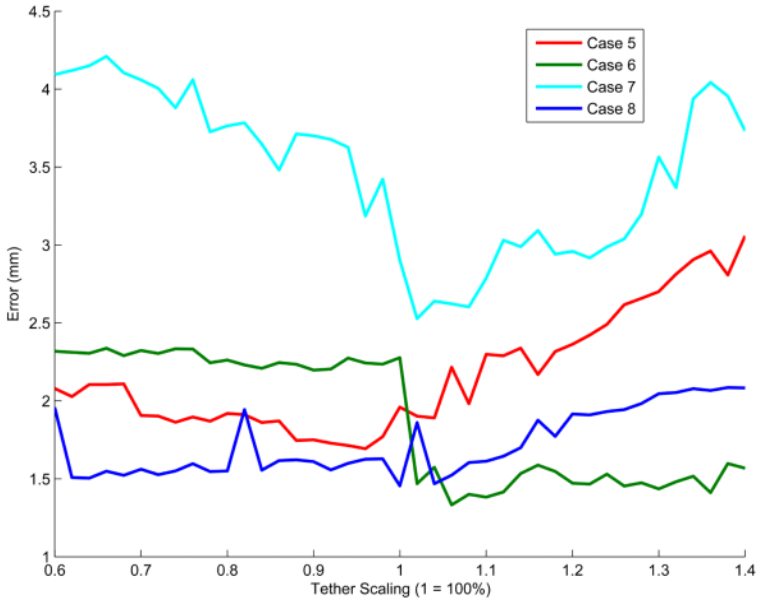

Figure 12.

Sensitivity of solution to tether lengths. The mean absolute prediction error (in mm) is shown as a function of various values of the tether lengths. In these plots, the x axis is a scaling factor multiplying the end diastole chordal length (EDCL), taken to be the distance between papillary muscles and chordal insertion points. A value of 1 corresponds to using the tether length at end diastole, other values of the *x*-axis correspond to multiplicative factors of the EDCL ranging from 0.6 to 1.4. These plots are interesting from a sensitivity analysis perspective, but they also inform the method as to the estimated patient-specific length of the chords, found as those that minimize the prediction error.

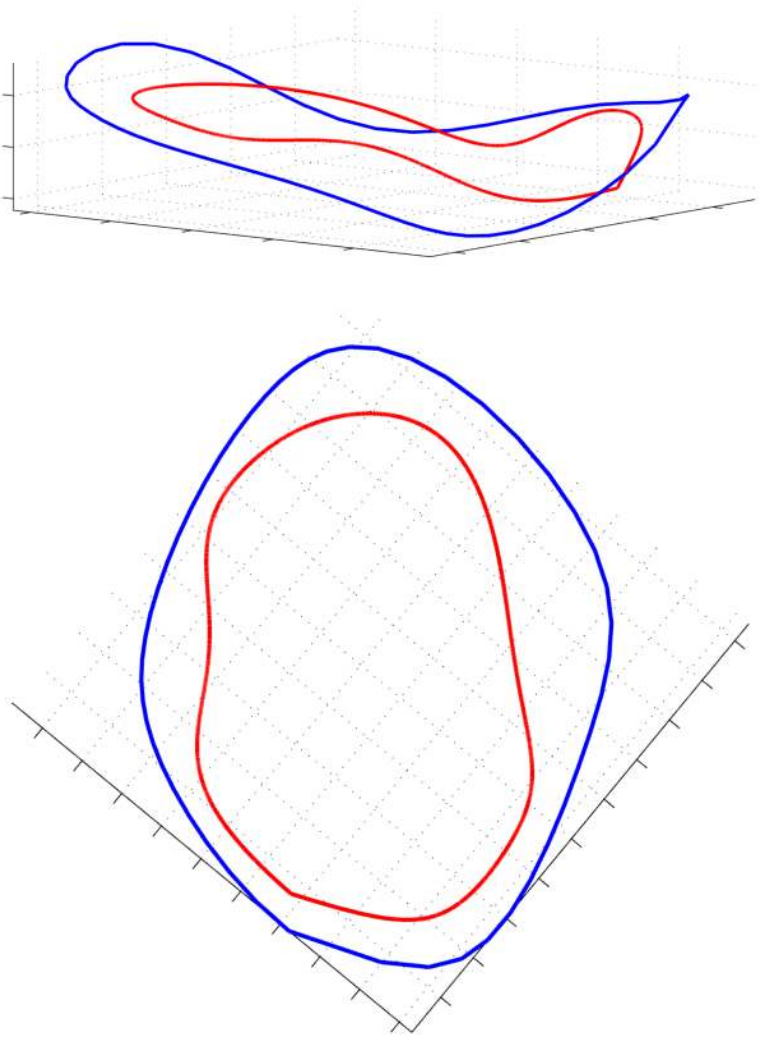

Figure 13.
Annulus at diastole and systole.

Table 1

TEE data characteristics: for each case study the table provides resolution, frame rate, depth, and image quality, as evaluated by a cardiologist: quality ranges from 1 - high quality/no artifacts, to 5 - poor quality/many artifacts

Case	Voxel Resolution (mm)	Frame Rate (Hz)	Ultrasound Depth	Image Quality
1	0.72×0.71×0.63	39	13	2
2	0.67×0.66×0.58	41	12	1
3	0.67×0.66×0.58	41	12	1
4	0.67×0.66×0.58	41	12	1
5	0.78×0.77×0.68	36	14	2
6	0.67×0.66×0.58	36	14	2
7	0.67×0.66×0.58	41	12	2
8	0.41×0.4×0.44	52	9	2
9	0.78×0.77×0.68	36	14	2
10	0.72×0.71×0.63	39	13	2

Table 2

Prediction error statistics. We compute the distance between ground truth closed configuration and predicted closed configuration meshes and report absolute error statistics in (mm). Columns from left to right indicate the mean absolute error, standard deviation, 5th and 95th per centile error values. Results are provided for optimal chordal length and labeled"(OPT)". The mean error for the case where the length was set as the assumed end diastole chordal length, taken to be the the distance, for the open valve, between papillary muscles head and chordal insertions, are provided on the right-most column and labeled "(EDCL)".

		(OPT)				(EDCL)
Case	**Patient**	**Mean**	**Std**	**5%**	**95%**	**Mean**
1	1	1.81	1.32	0.25	4.29	1.93
2	2	2.25	1.38	0.37	4.54	2.25
3	2	2.41	2.56	0.22	7.38	3.30
4	2	2.01	1.98	0.21	6.26	2.31
5	3	1.39	0.97	0.19	3.21	1.76
6	4	1.69	1.47	0.20	4.78	1.96
7	5	1.33	1.19	0.19	3.56	2.28
8	6	2.53	2.13	0.25	6.62	2.98
9	3	1.46	1.33	0.18	4.00	1.46
10	1	1.86	1.53	0.23	5.28	1.90
all	all	1.86	1.72	0.21	5.27	2.21